GL01223

ON THE THERMAL EFFECTS OF GROUNDWATER FLOW

1. REGIONAL SCALE SYSTEMS

Leslie Smith, Dept. of Geological Sciences,
University of British Columbia, Vancouver, Canada

David S. Chapman, Dept. of Geology and Geophysics,
University of Utah, Salt Lake City, Utah

H. Ross 5/1/82

This seems to be an excellent paper which could be a real contribution to the Thermal studies — groundwater literature. I have skimmed the paper (only) without recognizing any significant errors. I am unable to devote the time to a critical review for the next 10 da

submitted to

Journal of Geophysical

May, 1982

ABSTRACT

Numerical solutions of the equations of fluid flow and heat transport are used to quantify the effects of groundwater flow on the subsurface thermal regime. Simulations are carried out for a vertical section through a basin with a distance of 40 km separating the regional topographic high and low. Emphasis is placed on understanding the conditions under which advective effects significantly perturb the thermal field. The transition from conduction to advection dominated thermal regimes is sharp and depends primarily on the topographic configuration of the water table, the magnitude and spatial distribution of permeability, hydraulic anisotropy and depth of active flow. Deviations of surface heat flow from the background heat flux are a measureable effect of groundwater flow and depend on the same factors. Our results show that from zero to almost one hundred per cent of the section may have surface heat flow significantly different from background heat flow, depending upon the nature of the hydrogeologic environment. A limited spatial variability in a distributed set of heat flow measurements and/or linear temperature - depth profiles are not sufficient conditions to ensure that surface heat flow measurements are not disturbed. The results of our simulations suggest that knowledge of the complete environment of a site, including the water table configuration and subsurface flow system, combined with more closely spaced heat flow measurements may be necessary to unravel the true background heat flux in active flow regions.

INTRODUCTION

'Convection by groundwater in upper crustal rocks poses the greatest obstacle to determining from surface observations the heat flow associated with crustal conditions at depth' (Lachenbruch and Sass, 1977, p.648). This truism concerning the redistribution of heat by active groundwater flow systems, expressed by Lachenbruch and Sass (1977) in their recent evaluation of the thermal regime of the crust, has been of concern to heat flow investigators for as long as they have been making measurements. Van Orstrand (1934), Bullard (1939) and Birch (1947) in some of the earliest continental heat flow and thermal studies all found that purely conductive heat transfer processes were insufficient to explain observations of subsurface temperatures in drillholes. Groundwater motion, either in the formation, or within the drillhole itself, was cited as causing an advective perturbation to the otherwise conduction-dominated thermal regime. Many subsequent continental heat flow investigations based on a higher density of drillhole measurements, made with greater precision and finer sampling detail, have repeatedly confirmed this earlier observation (recent examples include, Lachenbruch et al., 1976; Lewis and Beck, 1977; Reiter et al.,1979; Brott et al., 1981; Chapman et al., 1981; Shearer and Reiter, 1981). In addition, the role of free and forced convection in controlling the thermal regimes within active hydrothermal systems in both continental and marine settings has become well established.

From a somewhat different approach, a number of groundwater hydrologists have also recognized the strong influence that

fluid flow has on the subsurface temperature distribution. These investigators have sought primarily to demonstrate this dependence (Stallman, 1963; Bredehoeft and Papadopulis, 1965; Parsons ,1970; Cartwright, 1971; Domenico and Palciauskis, 1973; Kilty and Chapman, 1980), to utilize this dependence as an aid in delineating the flow field (Bredehoeft and Papadopulos,1965; Cartwright,1970; Donaldson,1970; Sorey, 1971; Keys and Brown, 1978), to determine hydraulic properties (Bair and Parizek, 1979), or in prospecting for shallow aquifers (Cartwright, 1968; Kappelmeyer, 1957; Birman 1969)

It is recognized by both heat flow investigators and hydrologists who have studied thermal properties of flow systems that neither conductive nor advective heat transfer effects totally dominate the other for all surface geologic environments. Some regions, principally those stable tectonic areas with low topographic relief and relatively impermeable crystalline basement rocks at the surface appear to be conduction dominated. In contrast, both more permeable sedimentary basins and active tectonic zones of high topographic relief appear to contain regions of significant area in which the thermal regime is advection controlled. Hydraulic and thermal properties of basins and earth materials are such that conductive and advective terms in the heat transport equation can in some cases be of the same order of magnitude, and in other cases either term can dominate the other. An important corollary to this observation is that thermal fields are sufficiently sensitive to changes in measureable hydraulic and thermal parameters to make mathematical modeling of these

processes meaningful.

Review of Previous Work

The basic equations for transient heat transport in a fully saturated porous medium were given by Stallman (1960). Analytic solutions to these equations for simplified groundwater systems were subsequently developed by several authors. These solutions in turn are being superceded by quite general solutions to complex groundwater systems utilizing numerical techniques now available with large memory computers. It is useful here to review the evolution of models dealing with thermal aspects of groundwater flow, especially in terms of their use by hydrologists and geophysicists. Our interest here is with gravity-driven flow systems, rather than free convection. A descriptive and comparative summary of these papers is given in Table 1.

Perhaps the single most utilized analysis of thermal aspects of groundwater flow stems from the analytic solution for one dimensional (vertical) steady state flow of fluid between two points held at constant temperature, given by Bredehoeft and Papadopulos (1965). By matching the observed temperature profile to a set of type curves, the Darcy velocity of the fluid can be estimated. Minor modifications to this technique have been suggested by Stallman (1967) and Mansure and Reiter (1979). Examples of applying the method to field situations are found in Stallman (1967), Cartwright (1970), Sorey (1971), and Mansure and Reiter (1979). Popularity of this one dimensional solution is due in large part no doubt to its ease of application, and to

its apparent suitability in shallow recharge and discharge regions where flow may be largely vertical. Limitations of the analysis include the highly idealized flow system that it applies to, and the boundary conditions (discussed by Lachenbruch and Sass, 1977).

Another analytic solution for the temperature field, but for steady state flow in a rectangular domain with homogeneous, isotropic hydraulic conductivity is given by Domenico and Palciauskas (1973). The upper boundary of the flow field is the water table which is approximated by an analytic function. A principal contribution of the Domenico and Palciauskas (1973) analysis is in illustrating the important factors which control the temperature distribution in a given basin; namely thermal and hydraulic properties, and especially the geometry of the flow domain. Morgan et al. (1981) have recently applied this analytic solution to flow within basins of the Rio Grande rift, addressing specifically the permeability threshold at which forced convection thermal effects become significant.

There exists another class of studies, largely of two dimensional geometries, which solve for temperature distributions resulting from fluid flow. But in this case either the flow field or the temperature field of the moving fluid is assumed 'a priori'. Examples of this approach are papers by Lewis and Beck (1967) who assumed a uniform down-dip percolation of cold surface water to explain a well documented low heat flow pattern near Noranda, Quebec; Kilty and Chapman (1980) who assumed uniform velocities in identified aquifers to explain heat flow variations in three geologic settings including the

Hartville uplift in Wyoming,a Basin and Range forced convection geothermal system, and the Roan Antelope mine on the Zambian Copperbelt; and Brott et al. (1981) who assumed a constant velocity field within the Snake Plain aquifer to explain extensive temperature and heat flow data there.

These approaches also commonly include hybrid models where fluid flow is constrained to a specific region, such as a fracture, and the temperature field surrounding that region is assumed to be governed entirely by thermal conduction. Examples are the Bodvarsson (1969) analysis of temperatures within, and surrounding, a planar fracture, and Bodvarsson's (1972) solution for fluid temperatures upon radial injection into a confined aquifer. Keys and Brown (1978) use Bodvarsson's solutions to model temperatures observed during injection tests in the Ogallala Formation in Texas. Ziagos and Blackwell (1981) modify Bodvarsson's (1969) fracture temperature field for quite different boundary conditions, and demonstrate its applicability to transient thermal fields connected with shallow horizontal aquifers carrying discharge water from geothermal systems.

In defense of these latter approaches, it may be argued that hydrologic parameters are so poorly known as to make informed guessing of the groundwater velocity field a legitimate exercise. However, actual velocity fields are rarely as simple as assumed. A steady state flow system (Toth, 1962; Freeze and Witherspoon,1967) reflects the interplay of the topographic configuration of the water table, the ratio of the depth to lateral extent of the flow domain, and the spatial configuration of distinct permeability units. The rate of groundwater recharge

and discharge vary across the basin, even if the porous medium is homogeneous. Therefore although these simplified studies have considerable value in demonstrating thermal effects of specified velocity fields, it is desirable to attempt a proper solution for the flow field where possible.

Studies which address the more realistic problem of coupled groundwater flow and heat transport in heterogeneous, anisotropic media can be grouped into three categories according to their intended application. In one group are high-temperature reservoir simulations which deal with multiphase fluid and heat transport. These models are discussed in excellent reviews by Pinder (1979) and Garg and Kassoy (1981) and will not be summarized here. A second group, somewhat related to the first, deal with thermal energy storage in aquifers (eg. Lippman et al., 1977; Tsang et al., 1981; Sauty et al., 1982). A third group, most closely allied with our analysis, deal with low to moderate temperature geothermal systems in the framework of a groundwater flow system.

Parsons (1970) used a finite difference technique to solve the fluid flow and temperature equations in basins of arbitrary permeability and thermal conductivity configurations. The model was applied to both a hypothetical basin 320 m deep and 3.2 km wide with about 80 m of relief on the water table, and to a glacial complex in Northern Ontario. Emphasis was placed on replicating shallow temperature observations rather than on variations in surface heat flow caused by active flow regimes, although the latter are implicit in the results. Results indicated that fluid flow and thus temperature fields are

sensitive to permeability and water table configuration.

Sorey (1975,1976) has developed an algorithm utilizing integrated finite difference techniques. In an application to the thermal regime of Long Valley Caldera (Sorey, 1976) the transient temperature and flow regime was calculated for assumed fluid flux boundary conditions. The principal constraint for and emphasis of the study was the matching of discharge rates in thermal springs.

Using a finite element model, Betcher (1977) carried out a sensitivity analysis to investigate the effects of hydraulic conductivity, porosity, thermal conductivity and geothermal flux in determining the subsurface temperature distribution. The simulations considered a hypothetical basin 10 km wide and 2 km deep. However, in most of these simulations, no coupling was included between temperature, fluid viscosity, and fluid density.

Andrews (1978) and Andrews and Anderson (1979) have used finite element techniques to solve the time-dependent fluid and heat flow equations. Andrews (1978) considers local heating accompanying pumping from, and injecting into, a sandstone aquifer during operation of a heat pump system. Simulation results indicate again that temperatures are a sensitive measure of the pumping history of the wells, and that a superimposed regional groundwater flow can have significant effects in dissipating heat and in shifting temperature patterns. This model was also used to analyze thermal alteration of groundwater in the vicinity of a power plant cooling lake in Wisconsin (Andrews and Anderson, 1979).

There is ample evidence from this review (Table 1 and discussion above) that near surface thermal regimes are highly influenced by active groundwater flow systems. Geophysicists and hydrologists alike have used the sensitivity of temperature fields to groundwater velocities in order to exploit thermal measurements in terms of velocity fields and vice versa. What is less evident is the theoretical demonstration of the quantitative extent and spatial characteristics of the perturbation to surface heat flow to be expected given the existence of active groundwater flow systems.

In this study we address this question by utilizing numerical modeling techniques which permit consideration of fluid and heat transfer in heterogeneous, anisotropic media. Model output consists of the temperature field within and surface heat flow across a groundwater basin. Results are interpreted in terms of heat flow observations. Specific emphasis is placed on investigating the sensitivity of results to changes in permeability, hydraulic anisotropy, hydraulic gradient, depth of active flow, and configuration of and properties of aquifers. Subsequent papers will address the application of our model to a number of site-specific systems, and to thermal-hydrological effects on the local scale.

METHODOLOGY

Mathematical Model

The subsurface distribution of heat in a saturated porous medium can be described by two coupled differential equations;

one describing the fluid potential and the other temperature. In addition, equations of state are required to characterize the temperature dependence of fluid and medium properties. We use as a fluid potential an equivalent freshwater head, defined as:

$$h = \frac{p}{\rho_0 g} + z \qquad (1)$$

where p is fluid pressure, ρ_0 a reference fluid density defined for a fixed temperature, g the gravitational constant and z an elevation above datum. For the coordinate direction i, the fluid flux (specific discharge) is given by the equation:

$$q_i = -\frac{K_{ij}}{\mu}\left[\rho_0 g \frac{\partial h}{\partial x_j} + (\rho_f - \rho_0) g \frac{\partial z}{\partial x_j}\right] \qquad (2)$$

Here K_{ij} is the permeability tensor of the porous medium and μ the dynamic viscosity of the fluid. If we define a relative density

$$\rho_r = \frac{\rho_f}{\rho_0} - 1 \qquad (3)$$

then the fluid flux is given:

$$q_i = -\frac{K_{ij}\rho_0 g}{\mu}\left[\frac{\partial h}{\partial x_j} + \rho_r \frac{\partial z}{\partial x_j}\right] \qquad (4)$$

This equation represents two driving forces causing groundwater flow; piezometric head differences originating from the topographic relief on the water table and a buoyancy force due to density differences of the fluid.

In two dimensions, the steady state fluid continuity equation is given:

$$\frac{\partial}{\partial x}(q_x) + \frac{\partial}{\partial z}(q_z) = 0 \qquad (5)$$

Substitution of equation 4 yields the final form of the equation governing fluid flow:

$$\frac{\partial}{\partial x}\left[\frac{k_{ij}\rho_f \rho_o g}{\mu}\frac{\partial h}{\partial x}\right] + \frac{\partial}{\partial z}\left[\frac{k_{ij}\rho_f \rho_o g}{\mu}\frac{\partial h}{\partial z} + \frac{k_{ij}\rho_f \rho_o g}{\mu}\rho_r\right] = 0 \qquad (6)$$

Use of equivalent freshwater head rather than fluid pressure as the fluid potential is discussed by Bear(pp 654,1972) and Frind (1980). This approach has the advantage that the fluid flow equation is cast in terms of driving forces exclusive of static fluid pressure.

The heat transport equation describing the steady state temperature distribution in a saturated porous medium is given:

$$\frac{\partial}{\partial x}\left[(n\lambda^f_{xx} + (1-n)\lambda^s_{xx})\frac{\partial T}{\partial x} + (n\lambda^f_{xz} + (1-n)\lambda^s_{xz})\frac{\partial T}{\partial z}\right]$$
$$+ \frac{\partial}{\partial z}\left[(n\lambda^f_{zx} + (1-n)\lambda^s_{zx})\frac{\partial T}{\partial x} + (n\lambda^f_{ff} + (1-n)\lambda^s_{zz})\frac{\partial T}{\partial z}\right] \qquad (7)$$
$$- \rho_f C_f\left(q_x\frac{\partial T}{\partial x} + q_z\frac{\partial T}{\partial z}\right) = 0$$

where

T	temperature
C_f	specific heat of fluid
n	porosity

$\lambda^f_{xx}, \lambda^f_{xz}, \lambda^f_{zx}, \lambda^f_{zz}$ components of conduction-dispersion tensor, fluid

$\lambda^s_{xx}, \lambda^s_{xz}, \lambda^s_{zx}, \lambda^s_{zz}$ components of heat conduction tensor, solid

The first two terms in square brackets on the left hand side of the equation account for heat conduction and dispersion in the solid-fluid composite. The third term on the left hand side accounts for advection of heat with the fluid.

Components of the conduction-dispersion tensor include terms accounting for both heat conduction in the fluid and mechanical mixing due to unspecified heterogeneities within the porous medium. For an isotropic medium, the dispersion terms can be expanded as follows:

$$
\begin{aligned}
n\lambda^f_{xx} &= \rho_f C_f \left(\alpha_L q_x^2/\bar{q} + \alpha_t q_z^2/\bar{q} \right) + n\lambda^f \\
n\lambda^f_{zz} &= \rho_f C_f \left(\alpha_t q_x^2/\bar{q} + \alpha_L q_z^2/\bar{q} \right) + n\lambda^f \\
n\lambda^f_{xz} &= n\lambda^f_{zx} = \rho_f C_f (\alpha_L - \alpha_t) q_x q_z/\bar{q}
\end{aligned}
\qquad (8)
$$

Further discussion of dispersivity can be found in Bear (1972), Anderson (1979), and Sauty et al. (1982).

Equations 6 and 7 describe the movement of pure water as a single phase fluid. Both fluid flow and heat transfer are at steady state. No heat sources or sinks are considered and local thermal equilibrium between the porous medium and the fluid is required. Permeability, porosity, and thermal conductivity can vary in space. In solving this system of equations, we will assume that fluid density is a function of temperature but not pressure. Viscosity of the fluid will vary with temperature. Thermal conductivity is assumed to be independent of temperature and pressure, and porosity is not coupled to the fluid pressure.

An evaluation of the effects of temperature and pressure dependent thermodynamic and transport properties, in the context of free convection, is presented by Straus and Schubert (1977).

Several relationships are reported in the literature describing the dependence of fluid viscosity and density on temperature. We have chosen to use two of the more simple models, given as:

$$\mu = 2.4\times10^{-5} \times \left[10^{248.37/(T+133.15)}\right] \qquad (9)$$

$$\rho_F = \rho_0\left[1 - \beta(T-T_0) - \gamma(T-T_0)^2\right] \qquad (10)$$

$$\beta = 3.17\times10^{-4} \quad {}^{\circ}C^{-1}$$

$$\gamma = 2.56\times10^{-6} \quad {}^{\circ}C^{-2}$$

The viscosity equation was reported by Huyakorn and Pinder (1977), and the density equation by Sorey (1978). These relations are plotted in Figure 1.

The model we consider in this study is a vertical section through a groundwater basin. The upper boundary of the flow domain is the water table. Along this boundary the equivalent freshwater head is equal to the elevation of the water table above datum. Both impermeable or fluid flux conditions can be applied along the basin divides in the recharge and discharge area and along the basal boundary at depth. A known temperature distribution (either isothermal or determined from a lapse rate) is assumed for the water table. A heat flux is specified along the basal boundary. At the basin divides in the recharge and discharge areas, a condition of zero lateral heat flux and fluid flux is assumed.

The boundary conditions on the temperature field exert an important influence on the nature of our solutions. In specifying a basal heat flux, the subsurface temperature distribution will more closely reflect the influence of water table topography and fluid flow than it would if an isothermal basal boundary were assumed. Additionally, by utilizing a heat flux across the basal boundary, advection may alter the spatial distribution of heat flow but not it's mean magnitude (Ribando et al., 1976). By specifying a temperature everywhere along the water table, we implicitly assume that climate is the dominant control on shallow subsurface temperatures. This condition is somewhat restrictive in groundwater discharge regions because it does not account for local heating at the water table due to the upward flow of warmer water; nor does it account for the possible existence of thermal springs. Thermal gradients must adjust so that water advects across the water table at the specified temperature.

This study is restricted to media for which the hydraulic behavior can be characterized in a continuum sense. Such an approach is valid for granular porous media and fractured media with a high fracture density relative to the scale of the analysis. Table 2 is a summary table of permeabilities for common geologic media. Excluded from consideration are fracture networks of low density but with sufficient flow to warrant treatment as a set of discrete fractures.

In many of the examples to be presented, a subset of the fluid and thermal properties are not varied. The values assigned to these parameters are summarized in Table 3.

Numerical Solution

Equations 6 and 7 are solved numerically using a Galerkin finite element technique, with linear basis functions applied over triangular elements. The finite element grid we use in later simulations is shown in Figure 2. It is composed of 1260 elements and 688 nodes. A solution is obtained at the nodal points in the grid. Temperature varies linearly across each of the elements. A detailed development of the finite element method can be found in Pinder and Gray (1977). Examples of the application of finite element techniques to solve a variety of problems dealing with advective heat transport include Mercer et al. (1975), Andrews and Anderson (1979), and Li (1980).

The following procedure is used to couple the fluid flow and heat transport equations. Assuming first a conductive heat flow regime, appropriate densities and viscosities are calculated for each element in the grid using equations 9 and 10. The fluid flow equation is solved to obtain a set of equivalent freshwater heads at the nodal points, following which equation 4 is used to calculate a specific discharge (qx,qz) within each element. The average fluid velocity can be determined by dividing the specific discharge by the porosity assigned to that element. The heat transport equation is solved to determine a set of nodal temperature values. The density and viscosity of the fluid is updated for this new temperature field and an iterative sequence is entered in which the fluid flow and heat transport equations are solved successively until the maximum change in the nodal temperatures between iterations is less than a given tolerance. For the simulations reported here,

this tolerance is 0.1 °C.

Methods of Presenting Model Results

Figure 3 shows the form of graphical output and illustrates several general features of all models. This simple example simulates a basin 40 km wide, 5 km deep with a linear water table having a total relief of 500 m across the basin. No fluid flow occurs across the lateral and basal boundaries. An isothermal boundary is imposed at the upper surface and a constant heat flux at the lower surface; values of 20 C and 60 mW m^{-2} are used. The medium has a homogeneous and isotropic permeability. Results are shown for three different permeabilities: 1.0×10^{-18} m^2, 2.0×10^{-16} m^2, and 5.0×10^{-16} m^2. For illustrative purposes, all isotherm sections are plotted with a vertical exaggeration factor of 1.33.

Contoured isotherm sections are useful in demonstrating qualitative thermal effects. The upper section in Figure 3 illustrates one end member in which the specific discharge (and thus fluid velocity) is too small to have an effect on the conductive heat flow regime. We term this situation the 'conductive case'. Later we will examine in some detail the threshold conditions for which advective influences become significant. In the conductive case the isotherms must parallel the upper surface. The maximum temperature within the basin in this simulation is 149 °C (Figure 3), a condition governed entirely by the geometry of the basin, thermal conductivity of the saturated porous medium, and the basal heat flux imposed.

As permeability is increased, fluid velocities become

sufficient to redistribute heat in the system. Isotherms in the recharge area are depressed due to the downward flow of cooler water from the water table, whereas isotherms in the discharge region are elevated due to upward flow towards the water table. In the middle of the basin, isotherms are tilted with respect to their conductive configuration, but for a broad region they remain sub parallel to the surface indicating that heat flow variations across this region will be subdued even though an active groundwater flow system exists in the basin. Temperature changes at nodal points within the finite element grid vary from zero to about 15 °C in response to groundwater flow that accompanies a permeability change from 1.0×10^{-18} m^2 to 2.0×10^{-16} m^2. As permeability is increased further to 5.0×10^{-16} m^2, advective effects become clearly visible in the temperature cross section with a further depression of isotherms in the recharge area and a pronounced upwarp at the discharge area. Temperature changes with respect to the conductive case amount to about 40 °C in some extreme model simulations.

In addition to nodal temperatures, components of the heat flow vector can be calculated anywhere within the finite element grid. By convention, we shall refer to heat flow as the vertical component of of heat flux calculated using nodes at and immediately below the water table as 'surface heat flow'. The magnitude of surface heat flow and its spatial variation are important for several reasons. First, heat flow is a measureable quantity and thus serves as a test when applying models to specific situations. In this regard heat flow is a more fundamental quantity than the temperature distribution which is

significantly affected by thermal conductivity variations alone. Secondly, we will show that heat flow profiles can be used as diagnostic indicators of certain groundwater flow systems. Finally, a principal motivation for this study is the influence of groundwater flow on surface heat flow measurements and their interpretation.

Surface heat flow profiles calculated for the three cases of different homogeneous, isotropic permeability are shown in Figure 3. This plot is conceptually similar to one published recently by Morgan et al. (1981). In the purely conductive case of this example surface heat flow will be everywhere equal to the basal heat flux. For case a , which approaches the conductive case, heat flow lies everywhere between 59 and 62 mW m^{-2} compared to a basal heat flux of 60 mW m^{-2}. Increasing the permeability beyond the advective threshold increases the surface heat flow variability correspondingly. In case b, surface heat flow varies from 43 to 84 mW m^{-2}, with a root mean square deviation from the basal heat flux of 9.4 mW m^{-2}. In spite of this large variation, more than 60% of the basin has a surface heat flow within +/- 10% of the basal heat flux. In case c, the most disturbed case shown, overall surface heat flow variations are very large but 50% of the basin will still yield heat flow values within +/- 10% of the basal flux.

It is important to recognize the basis for, and limitations of, comparing our model results with field observations. Heat flow determinations are made by measuring temperature - depth profiles in drillholes, measuring thermal conductivity of representative samples in the laboratory, and then calculating

heat flow as the product of the conductivity and the temperature gradient (for details see Beck, 1965, or Kappelmeyer and Haenel 1974). We presume that sampling for thermal conductivity is sufficient to characterize the local geologic section, leaving as the principal uncertainty the determination of an appropriate gradient. Here common practice is somewhat arbitrary, especially when the gradient is neither constant in homogeneous material nor consistent with thermal conductivity changes in heterogeneous media. Figure 4, produced from simulation c in Figure 3, gives the computed temperature-depth distribution at the fourth column from the left in the finite element grid. This plot illustrates some of the difficulties in calculating surface heat flow. Temperature gradients vary from 15 to 20 °C per km within the upper 2 km at the site. If one were to assume that the gradient in the bottom portion of a drillhole is the most representative, then we have the unfortunate circumstance that the gradient and hence heat flow depends on the depth of a drillhole . A 100 m drillhole would yield a heat flow of 38 mW m^{-2},whereas 50 mW m^{-2} would be deduced in a 2000 m deep drillhole; neither value is in close agreement with the regional background heat flux of 60 mW m^{-2} imposed in the model.

Another practice sometimes used is to characterize the entire drillhole by a single thermal gradient, usually determined from a least squares fit of all available data in the undisturbed section of the borehole. Again in our example (Figure 4) the computed heat flow value changes with depth of investigation, in this analysis from 38 to 44 mW m^{-2} utilizing progressively more data. The most rigorous treatment of data

such as these (Mansure and Reiter, 1979) addresses the implied one-dimensional downward vertical flow, but that is contingent upon recognizing the systematic trend of increasing gradients in the data. It is doubtful whether the example shown, in which the gradient changes from 15.5 °C/km for the uppermost 100 m to 16.6 °C/km for the interval 400 to 800 m, would be recognized as such, even though the calculated heat flow deviates by 37 % from the background flux.

For consistency in our model results, we always compute the temperature gradient over a 100 m depth interval immediately below the water table. The results therefore should ideally be compared with field results over the same interval. In as much as field determinations of heat flow in deeper investigations are consistent with shallower results, they too will be comparable. When discrepancies do exist between heat flow calculated for the uppermost 100 m of the borehole and calculated in deeper sections, our model results will be 'worst case examples' because heat flow results from deeper investigations tend towards the background flux.

It should also be recognized that surface heat flow as used here refers only to conductive heat flow across the water table. The advective transfer of heat across the water table with the recharging and discharging groundwater is not included in the calculation of surface heat flow. Because of an assumed isothermal upper boundary, the net advective transfer of heat will be zero. However, the spatial variation in this component will vary with the spatially distributed rate of groundwater recharge and discharge. For all simulations reported in this

paper, advective heat transfer is a minor component of a total heat budget at the water table, even in 'hydrologically disturbed' cases. Only when the fluid flux across the water table is strongly focussed in a small proportion of the total basin width is the advective heat transfer a significant fraction of the conductive transfer.

RESULTS

We now present results from simulations which systematically explore the following effects: (a) variable but homogeneous isotropic permeability, (b) anisotropic permeability, (c) water table topography , and (d) aquifer geometry and properties. Output data for all models consists of equivalent fresh water head and temperature values for all nodes in the finite element grid. From this data, isotherm sections, vertical temperature and temperature gradient plots, and surface heat flow profiles are constructed.

The flow domain we consider is a two-dimensional section 40 km wide and 5 km deep. The water table is represented by three linear segments simulating upland, slope and lowland regions respectively. The upland and lowland regions are characterized by a water table gradient of 17.2 m per km. The water table gradient of the slope connecting these two segments is 51.6 m per km. Total relief on the water table is 1 km. This geometry matches foothill topography typical of Eastern and Western North America and at the same time simulates subdued Basin and Range terrain from which we will draw some feld examples.

A basal heat flux of 60 mW m^{-2} is used for all models.

The thermal effects of groundwater moving through a porous medium with a homogeneous permeability are illustrated in Figures 5 and 6. The temperature field and the surface heat flow profile now have a new character resulting from the segmented water table topography which did not appear in the linear water table example discussed in the methods section. In particular there is no longer a monotonic increase in surface heat flow from the recharge region to the discharge region. We now see a more even heat flow deficit across the uplands recharge region with a local minimum at the top of the slope, caused partially by a conductive topographic effect (Lachenbruch, 1969) but more importantly by enhanced downward fluid flow in response to topography. Heat flow rises rapidly down the slope as the thermal regime is affected by an upward component in the fluid flow. In the lowlands region, heat flow again exhibits more of a plateau than in the linear water table case. A local maximum now exists at the toe of the slope. Overall maximum heat flow is observed at the lowest elevation in the basin. Three examples in Figure 5 illustrate purely conductive effects, minor advective effects, and severe advective effects.

The evolution from a conductive regime to a thermal regime dominated by the effects of groundwater flow is shown more clearly in Figure 6. Here we have chosen six characteristic sites in the model, described in Table 4, and trace surface heat flow at each of these sites as permeability is systematically altered. Such a display yields a striking illustration of the permeability threshold for the redistribution of heat by advection.

Continental heat flow, with the exception of geothermal areas, varies from about 35 mW m^{-2} on shields to 120 mW m^{-2} in tectonically active areas, but 60 mW m^{-2} is near the modal value for continents as reported by Jessop et al. (1976) on the basis of heat flow determinations published at that time. We have run otherwise identical models with heat flow values of 40 , 60, and 80 mW m^{-2}. Although the surface heat flow perturbations do not scale exactly linearly, all important effects are evident in the 60 mW m^{-2} case.

Unless otherwise noted, porosity decreases with depth in a piecewise manner from 0.20 at the surface to 0.02 at the base of the model. Although a uniform solid-matrix thermal conductivity is used, the rock-fluid mixture conductivity varies with porosity (and hence depth) according to the relation (Bear, 1972):

$$\lambda_x = n\lambda^f + (1-n)\lambda^s_{xx}$$
$$\lambda_z = n\lambda^f + (1-n)\lambda^s_{zz} \qquad (11)$$

Little guidance is available in selecting values of the longitudinal and transverse dispersivity for a flow system of this scale. Values of 100 m and 10 m are used as likely representative of an upper range of possible values. A series of model runs in each of the cases to be presented shows that with dispersivities of this magnitude, mechanical dispersion is a minor component of the conduction-dispersion tensor and results are not sensitive to these assumed values.

Case 1. Homogeneous permeability

The thermal effects of groundwater moving through a porous medium with a homogeneous permeability are illustrated in Figures 5 and 6. The temperature field and the surface heat flow profile now have a new character resulting from the segmented water table topography which did not appear in the linear water table example discussed in the methods section. In particular there is no longer a monotonic increase in surface heat flow from the recharge region to the discharge region. We now see a more even heat flow deficit across the uplands recharge region with a local minimum at the top of the slope, caused partially by a conductive topographic effect (Lachenbruch, 1969) but more importantly by enhanced downward fluid flow in response to topography. Heat flow rises rapidly down the slope as the thermal regime is affected by an upward component in the fluid flow. In the lowlands region, heat flow again exhibits more of a plateau than in the linear water table case. A local maximum now exists at the toe of the slope. Overall maximum heat flow is observed at the lowest elevation in the basin. Three examples in Figure 5 illustrate purely conductive effects, minor advective effects, and severe advective effects.

The evolution from a conductive regime to a thermal regime dominated by the effects of groundwater flow is shown more clearly in Figure 6. Here we have chosen six characteristic sites in the model, described in Table 4, and trace surface heat flow at each of these sites as permeability is systematically altered. Such a display yields a striking illustration of the permeability threshold for the redistribution of heat by advection.

For permeabilities less than 1.0×10^{-17} m^2 the thermal regime is entirely conductive and surface heat flow almost everywhere is equal to the basal heat flux in the model. Exceptions are sites c and d (Figure 6) at the breaks in slope of topography. Heat flow at these sites for the low permeability cases are 57 and 63 mW m^{-2}, in close agreement with values computed by other means (Lachenbruch, 1969) for the two dimensional conductive heat flow topographic effect.

For permeabilities greater than 1.0×10^{-17} m^2 the thermal regime is increasingly affected by groundwater flow. However the severity of the heat flow redistribution depends on position in the basin. From Figure 6 it can be seen that intermediate sites on the upland and lowland plains (sites B and E) are least affected over much of the permeability range. Sites A, C and D at the recharge divide and at the breaks in slope are affected to a greater degree while site F at the discharge divide is most affected. Furthermore, the advective influence on heat flow can be very large in one part of the system while moderate elsewhere. The reversal in slope of curve D is not significant here. For permeabilities less than 8.0×10^{-16} m^2, the local maximum in surface heat flow is centered in the grid element at D. However, at the higher permeability value, this local maximum is displaced downstream slightly, yielding an apparent reduction in the heat flow disturbance.

The lateral variability in surface heat flow is often used as an indicator of the presence or absence of groundwater flow. However, it is important to recognise that large parts of this system , sites A to C and D to E (Figure 6), can yield surface

heat flow values which vary along profile by only a few percent, while the measured value may be quite different from the basal flux. With respect to heat flow anomalies, two classes of effects are observed in the model: a transition from one level of heat flow to another as occurs from the top of the slope to the toe of the slope for the segmented water table, and secondly, a peak such as occurs at the lowest elevation in the basin. These anomalies are governed by the groundwater flow system and especially by the water table geometry, but may be mistaken as indicators of deeper but spurious thermal processes in the crust.

The temperature dependence of fluid density and fluid viscosity are important effects in determining the deviation of surface heat flow from the background heat flux. Two simulations are carried out in which first fluid density and then fluid viscosity are constant with values calculated using the temperature at the water table. In these simulations, the medium permeability is 8.0×10^{-16} m^2, representing a disturbed case. For the fully coupled analysis considered in previous paragraphs, the root mean square deviation of surface heat flow as compared to the basal heat flux is 49.3 mW m^{-2}, with a maximum surface heat flow of 216 mW m^{-2}. If fluid density is constant (all buoyance terms are zero), and viscosity is coupled to temperature, the temperature distribution and surface heat flow are very similar to the fully coupled problem except in the region between 30 and 40 km (Figure 5). In the uncoupled case, isotherms are not upwarped as much as in the coupled problem. The dq rms value is 44.3 mW m^{-2} with a maximum surface heat flow

of 177 mW m^{-2}.

A more dramatic effect is observed if fluid viscosity is constant. The hydrologic disturbance is effectly damped throughout the section, with a dq rms value of 17.0 mW m^{-2}. The maximum surface heat flow is 90.7 mW m^{-2}. It is probable that the reduced fluid viscosity at depth due to higher temperatures promotes deeper circulation of groundwater which can enhance the hydrologic disturbance. Thus, the decrease in viscosity with depth has the effect of shifting the advective theshold towards lower permeability values, relative to the uncoupled case.

The permeability threshold for heat redistribution also depends upon the hydraulic gradient. Discussion of a permeability threshold cannot be divorced from consideration of the water table configuration. In this study we have chosen to work primarily with one basin, as shown in the Case 1 simulations. However, it is instructive to document the effect of varying the topographic relief on the water table. A series of simulations have been carried out for two additional water table configurations. In one set, the slope on each segment of the water table is decreased by a factor of 1.5 and in the second set, the slope is increased by a factor of 1.5, relative to the case previously discussed. Total relief on the water table across the basin is 0.67 km and 1.5 km, respectively. Permeability is assigned the values 1.0 x 10^{-16} m^2, 3.0 x 10^{-16} m^2, and 8.0 x 10^{-16} m^2. Porosity is constant with a value 0.05.

Table 5 summarizes the effect of the water table slope. The root mean square deviation of surface heat flow as compared to the basal heat flux is taken as a measure of the degree of

hydrologic disturbance. With a greater relief on the water table, the hydraulic gradient increases and advective effects on heat redistribution are strengthened. This response will have the effect of shifting the threshold value towards a lower permeability.

Case 2 Homogeneous, anisotropic permeability

Porous media commonly exibit an anisotopic permeability. On a regional scale, anisotropic ratios (kx/kz) of up to 100:1 can occur due to the effects of layered heterogeneities within sedimentary units or volcanic flows (Freeze and Cherry, 1979). This ratio is much greater than that which is observed on the scale of a rock core. Anisotropy ratios kx/kz probably vary between 1:1 and 100:1 for the scale of problem we are considering. In fractured rock, it is possible that the vertical permeability may be greater than the horizontal permeability. Such would be the case if, for example, there were greater frequencies or larger aperatures associated with a vertically-directed set of joints or fractures. This possibility will be discussed later in Case 5. The analysis in this section applies to media with a greater horizontal permeability than vertical permeability. The concept of a permeability threshold for heat redistribution must be cast in light of the tensorial nature of permeability.

Figure 7 illustrates the effects of anisotropy on heat flow for the case where the horizontal permeability kx is 8.0×10^{-16} m^2 and kz is reduced by a given factor. In the most permeable case shown, and for the isotropic end member, the heat flow

profile includes slope-induced local maxima and minima, heat flow plateaus in the recharge and discharge regions and a large peak at the principal discharge divide. Only six percent of the length of the profile has a surface heat flow within 20% of the basal flux. Increasing the anisotropic ratio kx/kz to 10:1 eliminates local effects including plateaus and reduces the discharge maximum by a factor of two. A further increase of the anisotropic ratio kx/kz to 100:1 produces an extremely subdued surface heat flow profile where all values fall between 52 and 67 mW m^{-2}.

The effects of anisotropy on the thermal regime of the basin are twofold: deviations from the basal flux are subdued, and local maxima and minima along the heat flow profile associated with the top and toe of the water table slope are eliminated. The explanation for both effects lies in an increased difficulty of moving groundwater vertically downward or upward under a reduced value for the vertical permeability. In addition, pathlines for fluid flow are deflected toward the direction of maximum permeability, in this case concentrating more of the flow at shallower depths.

The influence of anisotropy over a range of permeability values is summarized in Figure 8. Increasing the anisotropy both decreases the magnitude of the hydrologic disturbance substantially for a given permeability, and also increases the threshold for the horizontal permeability at which advective effects dominate conductive effects. For example, if a dq rms of 6 mW m^{-2} (10% of the basal heat flux) is taken to mark the advective threshold, then an increase in the anisotropic ratio

kx/kz from 1 to 100 corresponds to a shift in the threshold for the horizontal permeability from 7.0×10^{-17} m^2 to 9.0×10^{-16} m^2. In other words, a large scale anisotropy due to layered heterogeneity permits surface heat flow measurements to be made over a broader range of permeabilities before encountering serious advective effects.

Case 3. Effect of the Depth of the Basin

We have thus far demonstrated the effects of the magnitude of permeability and anisotropy on temperature regimes within a basin with a fixed geometry, 5 km deep at its recharge end. We now consider the thermal consequences of restricting active groundwater flow to progressively shallower depths. These simulations are accomplished by establishing a very low permeability value (equal to 1.0×10^{-21} m^2) for all elements below a selected depth, and by setting various homogeneous isotropic conditions for the medium between the surface and that depth.

Surface heat flow profiles for a basin with four different depth restrictions, but all having an upper medium permeability of 8.0×10^{-16} m^2 are given in Figure 9. Effects of restricting the depth of flow are significant. Heat flow perturbations are greatest for the deepest flow regime and decrease in magnitude as the depth of active flow is restricted. However the local maxima and minima associated with the breaks in the water table slope are not progressively smoothed. Surface heat flow at the toe of the slope (site d, Table 4) appears to be particularily sensitive to changes in the depth of flow. The wavelength of

perturbation effects does not change with progressively shallower flow because it is governed by the water table topography. Figure 10 shows the quantitative effects of depth of flow for a range of upper layer permeabilities and four different flow depths. Restricting the active flow in our 5 km deep basin to the upper 2 km in a medium of permeability 8.0 x 10^{-16} m^2 reduces the dq rms value from 55 to 5 mW m^{-2}. For a lesser permeability of 3.0 x 10^{-16} m^2 the corresponding reduction in dq rms is from 21 to 2.4 mW m^{-2}. Decreasing the depth of flow shifts the advection threshold toward higher permeability values. In this case the threshold permeabilities (isotropic) corresponding to a decrease in the circulation depth from 5 to 2 km shifts from 7.0 x 10^{-17} to 9.0 x 10^{-16} m^2.

The increase in the permeability threshold due to both anisotropy and restricted flow depth together provides a possible explanation for an apparent discrepancy between model results and field observations. The discrepancy arises because predominantly conductive heat flow determinations are commonly made in some sandstones, fractured crystalline rocks and unconsolidated deposits having permeabilties ranging from 1.0 x 10^{-17} m^2 to 1.0 x 10^{-15} m^2 (see Table 2). However model results for the homogeneous, isotropic, 5 km deep basin (cases b and c of Figure 5; Figure 6) suggest that the thermal regime for much of this permeability range should be dominated by advective effects. It appears that either a large-scale anisotropy or a decrease in depth of flow shifts the threshold for horizontal permeability separating conductive from advective dominated thermal regime by about an order of magnitude. We have simulated

the combined effects for a flow depth of 2 km and anisotropic ratio kx/kz equal to 100:1, and find that the permeability kx can rise to 3.0×10^{-15} m^2 before dq rms exceeds 10% of the basal heat flux, and to 5.0×10^{-15} m^2 before it exceeds 20%. These latter permeabilities are well within the range expected in the field and thus the apparent discrepancy may be resolved.

Case 4. Effect of Aquifers

Although basins with a homogeneous permeability are instructive to study because of their relative simplicity, it is more common to have heterogeneous permeability distributions. Both layered sedimentary rock sequences and volcanic flow fields exhibit permeabilities covering much of the range for geologic media given in Table 2. The systems are commonly layered, the layering being sub-horizontal in undeformed terrains, otherwise tilted or offset. In this section we will restrict our investigations to layered media, and consider the thermal effects of horizontal aquifers only. Specific parameters of interest are aquifer depth, thickness, and permeability.

Figure 11 shows the effect of a single horizontal aquifer, 350 m thick, having a permeability 1.0×10^{-14} m^2 within a medium less permeable by a factor of 100. This aquifer permeability characterizes that of permeable sandstones, limestones, and some basalt flows (see Table 2). The principal thermal effect of the aquifer is to depress isotherms and hence surface heat flow rather uniformly in the recharge or upland region and to raise isotherms and elevate heat flow in the lowlands. As shown by simulations a, b, and c in Figure 11, when

the aquifer is deeper in the flow system the hydrologic disturbance becomes more severe. This effect has a similar explanation to that for the homogeneous basin with varying depth of active flow. Deep aquifers promote deep circulation patterns into regions of higher temperature and leads to a greater departure from conductive thermal conditions throughout the basin.

A summary of several effects are shown in Figure 12. Here we vary the depth of the aquifer, the thickness of the aquifer, and the permeability contrast between the aquifer and the surrounding medium which is assigned a permeability of 1.0×10^{-16} m^2. The hydrologic effect is again measured by dq rms, the root mean square deviation of surface heat flow from the basal heat flux. As expected, the hydrologic disturbance increases with greater aquifer depth, with greater aquifer thickness and with greater aquifer permeability. The magnitude of the disturbances in Figure 12 suggest that great caution should be exercised when making heat flow measurements in such geologic terrains. In particular it is important to recognize if and when the thermal regime is being controlled by a more permeable unit at depth, and to know how field observations in disturbed cases relate to the background heat flux.

Figure 13 shows temperature-depth and gradient-depth plots characteristic of different sites across one such basin containing a prominent aquifer. At each site the profiles penetrate through the aquifer. Near surface thermal gradients are depressed in the recharge areas but are elevated in the discharge areas. The slowly changing gradients or equivalently

the curved temperature profiles above the aquifer are diagnostic of vertical groundwater flow as has been shown for the one-dimensional situation (Bredehoeft and Papadopolis, 1966; Sorey, 1971). It can also be seen from Figure 13 that temperatures are not isothermal within the aquifer at any location, nor are they isothermal along the length of the aquifer. Gradients may increase (site a), remain constant (site b), or decrease (site c) within the aquifer, depending on the site location in the basin. Another important observation from these steady state simulations is that the gradient and hence heat flux below the aquifer is constant at all sites and is equal to the basal heat flux. The linear portions of these temperature profiles can therefore be used to determine reliable regional heat flow values.

The temperature-depth profiles can be exploited further to yield information on the groundwater flow system. Zero-depth or surface intercept temperatures in purely conductive thermal regimes will always be equal to the water table temperature. However surface temperatures at the three sites in Figure 13, extrapolated from the linear portions of the temperature profiles below the aquifer are 7, 20, and 32 °C for sites a, b and c respectively, compared to a constant water table temperature of 20 °C. Extrapolated surface temperatures thus exceed actual surface temperatures in discharge regions, and underestimate actual surface temperatures in recharge zones. The mismatch between actual and extrapolated surface temperatures may then be a good indicator of site location with respect to the groundwater flow system.

The perturbation of the conductive thermal regime due to the presence of a confined aquifer depends strongly on the permeability of the surrounding medium in which the aquifer is embedded. This effect is shown in Figure 14 for simulations of an aquifer 350 m thick and permeability 1.0×10^{-14} m^2 embedded in three different media having lower permeabilities by factors of 0.03, 0.005, and 0.001 respectively. Hydrologic disturbances are progressively diminished in the three simulations. The aquifer embedded in a very low permeability medium has little effect on the conductive thermal regime, due to the difficulty of providing recharge into and discharge from the aquifer.

Case 5. An Additional Example.

Our final simulation combines many features previously investigated separately into a single model. The permeability distribution (Figure 15) has been arranged to simulate a basin with the following properties: (1) a relatively permeable vertical recharge zone at the highest elevation region as might occur in a volcanic pile or when an aquifer crops out at high elevation, (2) a thin aquifer at a depth of 2 km which is offset vertically in two regions, and (3) a low permeability layer overlying the aquifer in the left hand side of the grid. Offsets in the aquifer might simulate, for example, a series of normal faults at the topographic break in slope for the left offset, and a horst structure for the right offsets. The permeability distribution shown in Figure 15 is in general characteristic of many Basin and Range systems, although permeabilities of individual components of the section may vary considerably and

will ultimately govern details of the thermal regime. Porosity decreases from 0.2 at the surface to 0.1 for the lowermost elements.

The topographic relief on the segmented water table is again 1 km across the 40 km basin, but rather than having an isothermal upper surface boundary condition we assign the water table a variable temperature; 20 °C at the lowest elevation and decreasing by a lapse rate of 7 °C per km of elevation increase to the highest elevation. Basal heat flux is 60 mW m^{-2} as before.

Figure 15 shows results of the simulation including the temperature field, surface heat flow profile, and three temperature-depth and gradient-depth plots. Isotherms are severely depressed in the dominant recharge area, leading to surface heat flow values less than one quarter of the background flux. Isotherms elsewhere reflect the vertical geometry of the aquifer.

Heat flow values determined at sites above the low permeability layer vary systematically from 25 to 65 mW m^{-2}. However in contrast to case 3 (previous section) where non-linear temperature profiles could be taken as indicators of hydrologic disturbances, in this simulation the temperature-depth plots are linear and gradients are constant above the aquifer. Boreholes for heat flow studies at these sites will yield apparenty conductive heat flow values based on temperature-depth data down to depths of 2 km, but the values would deviate from the background flux by up to 60%. Furthermore, boreholes of 1000 to 2000 m depth will yield the

same spurious regional heat flux values as boreholes only 100 m deep. Without drillholes exceeding 2500 m at sites a and b and 3000 m at site c (Figure 15), the correct basal heat flux could not be determined from an isolated borehole. As in the previous case, thermal gradients below the aquifer are constant and equal at all sites.

The offset of the aquifer at the lower end of the flow system (Figure 15) produces an upwarp in the isotherms and a local asymmetric heat flow maximum. Surface heat flow in the discharge region attains a value twice background.

This model also provides the opportunity to investigate the effects of a greater vertical than horizontal permeability in the uppermost region of the recharge area. Unlike the anisotropic media discussed in case 2, this condition can lead to greater downward flow of water, increasing the disturbance of the conductive thermal regime. With the horizontal permeability of the vertical recharge zone equal to 8.0×10^{-16} m^2 as in the earlier simulation, several model runs are carried out with the vertical permeability increased by factors of 5, 10, and 20. Surface heat flow relative to the isotropic case (Figure 15) is slightly lower throughout the region from 0 to 23 km and slightly higher from 23 to 40 km. The root mean square deviation of surface heat flow from background in these three examples is 33.4, 34.1, and 34.6 mW m^{-2}; respectively. In the isotropic case, the dq rms is 29.5 mW m^{-2}. This behavior is conditioned on the fact that the horizontal permeability in the recharge zone exceeds the advective threshold. A more dramatic change in dq rms would occur if the vertical permeability were increased.

through the advective threshold for a case where both the horizontal and vertical permeability are initially below the threshold.

Simulations of this form, drawn on quite plausible permeability distributions, may provide a partial explanation for the considerable variability in heat flow values in continental regions of high topographic relief. Heat flow sites are seldom spaced more closely than 10 km, and it would not be uncommon to have just one site along the profile shown in Figure 15 with the purpose of determining the regional heat flux. The simulations further suggest that a knowledge of the complete environment of a site, including water table configuration and subsurface flow, combined with more closely spaced heat flow determinations may be necessary to unravel the true background heat flux in such situations.

CONCLUSIONS

Numerical modeling of the combined effects of fluid flow and heat transport can be used to quantify the effects of groundwater flow on the subsurface thermal regime in a basin. Two dimensional simulations of a basin 40 km wide and 5 km deep with 1 km of relief on a segmented water table lead to the following conclusions:

1. At a low permeability limit (permeabilities less than 5.0×10^{-17} m^2 for the basin investigated) the thermal regime of the region is purely conductive. Groundwater flow velocities are too small to effect significant redistribution of heat by advection.

2. The transition from a conduction dominated to an advection dominated thermal regime is sharp, occurring over a permeability range less than one order of magnitude, although geologic media exhibit a total permeability range of at least thirteen orders of magnitude. The threshold at which advection becomes important occurs at a permeability of 7.0×10^{-17} m^2 for the specific basin geometry studied and with a homogeneous, isotropic medium.

3. Thermal regimes, when advective effects are significant, are affected by topographic configuration of the water table, magnitude and spatial distribution of permeability, hydraulic anisotropy and depth of active flow. Increasing the hydraulic anisotropy to 100:1 (kx/kz) or reducing the depth of flow from 5 km to 2 km can extend the advective threshold for horizontal permeability by a factor of 15. In the basin modeled, a combination of high anisotropy and shallow depth of active flow raises the conduction-advection threshold for horizontal permeability from 7.0×10^{-17} m^2 to 3.0×10^{-15} m^2.

4. Hydraulic anisotropy such as would be expected in horizontally layered sedimentary units reduces advective perturbations to the thermal regime and smooths the surface heat flow profile.

5. As the depth of active flow is reduced, advective perturbations to the thermal regime are reduced. Local effects at breaks in slope of the water table can have a more complex dependence on the depth of flow.

6. Aquifers produce significant perturbations to the thermal field of a basin, but only if the permeability of the

surrounding medium is great enough to permit adequate recharge to and discharge from the aquifer. Thermal perturbations increase as the aquifer permeability or thickness increases and as the aquifer depth increases.

7. Computed temperature-depth profiles through aquifers indicate that aquifers are not isothermal. They may have increasing, constant, or decreasing thermal gradients within them depending upon location in a basin. Linear temperature-depth profiles immediately below an aquifer however will yield the correct background heat flux if the thermal regime of the basin is at steady state. If low permeability rocks overlie part of an aquifer, the thermal regime within the aquitard will be conduction dominated with a constant gradient throughout, but the heat flow deduced in these units may depart significantly from the background flux.

8. The thermal regime within a basin with spatially varying permeability, and with a structurally controlled system of aquifers will be complex. Caution should be exercised when interpreting heat flow results in such regions as regional heat flow values. A series of shallow drillholes along the hydraulic gradient would probably yield more information about the thermal regime than would one deep drillhole, unless the deep hole penetrated through the deepest aquifer. Plotting of heat flow sites in terms of their position in the groundwater flow system would be a useful convention to adopt, if advective effects are suspected.

ACKNOWLEDGEMENTS

This research was supported initially on a Department of Energy grant DE-AC07-80ID-12079. Acknowledgement is made to the Donors of the Petroleum Research Fund, administered by the American Chemical Society, for the partial support of this research.

REFERENCES

Anderson, M.P., Using models to simulate the movement of contaminants through groundwater flow systems, CRC Critical Reviews in Environmental Control, 9(2), 97-156, 1979.

Andrews, C.B., The impact of the use of heat pumps on ground water temperatures, Ground Water, 16(6), 437-443, 1978.

Andrews, C.B., and M.P. Anderson, Thermal alteration of groundwater caused by seepage from a cooling lake, Water Resour. Res., 15(3), 595-602, 1979.

Bair, E.S., and R.R. Parizek, Detection of permeability variations by a shallow geothermal technique, Groundwater, 16(4), 254-263, 1978.

Bear, J., Dynamics of Fluids in Porous Media, Elsevier, 1972.

Beck, A.E., Techniques of measuring heat flow on land, in Terrestrial Heat Flow, Geophysical Monograph 8, edited by W. Lee, pp24-50, AGU, Washington, D.C., 1965.

Betcher, R.N., Temperature distribution in deep groundwater flow systems - a finite element model, M.Sc. thesis, Univ. of Waterloo, 1977.

Birch,F., Temperature and heat flow in a well near Colorado Springs, Am. J. Sci.,245, 733-753, 1947.

Birman, J.H., Geothermal exploration of ground water, Geol. Soc. Am. Bull., 80, 617-630, 1969.

Bodvarsson, G., Thermal problems in the siting of reinjection wells, Geothermics, 1(2), 63-66, 1972.

Brott, C.A., D.D. Blackwell, and J.P. Ziagos, Thermal and tectonic implications of heat flow in the Eastern Snake River Plain, J. Geophys. Res., 86, 11709-11734, 1981.

Bullard, E.C., Heat flow in South Africa, Proc. Roy. Soc. London, A173(995), 474-502, 1939.

Bredehoeft, J.D., and I.S. Papadopulos, Rates of vertical groundwater movement estimated from the earth's thermal profile, Water Resour. Res., 1(2), 325-328, 1965.

Cartwright, K., Thermal prospecting for groundwater, Water Resour. Res., 4(2), 395-401, 1968.

Cartwright, K., Groundwater discharge in the Illinois Basin as

suggested by temperature anomalies, Water Resour. Res., 6(3), 912-918, 1970.

Cartwright, K., Redistribution of geothermal heat by a shallow aquifer, Geol. Soc. Am. Bull., 82, 3197-3200, 1971.

Chapman, D.S., Clement, M.D. and C.W. Mase, Thermal regime of the Escalante Desert, Utah, with an analysis of the Newcastle Geothermal System, J. Geophy. Res., 86(B12), 11735-11746, 1981.

Domenico, P.A., and V.V. Palciauskas, Theoretical analysis of forced convective heat transfer in regional groundwater flow, Geol. Soc. Amer. Bull., 84, 3803-3814, 1973.

Donaldson, I.G., Temperature gradients in the upper layers of the earth's crust due to convective water flows, J. Geophys. Res., 67, 3449-3459, 1962.

Freeze, R.A., and J.A. Cherry, Groundwater, Prentice Hall, 1979.

Freeze, R.A., and P. Witherspoon, Theoretical analysis of regional groundwater flow: 2. Effect of water table configuration and subsurface permeability variation, Water Resour. Res., 3, 623-634, 1967.

Frind, E.O., Seawater intrusion in continuous coastal aquifer - aquitard systems, Proc. Third Inter. Conf. on Finite Elements in Water Resources, Univ. Miss.,Oxford, May, 1980.

Garg, S.K., and D.R. Kassoy, Convective heat and mass transfer in hydrothermal systems, in Geothermal Systems - Principles and Case Histories, edited by L. Rybach and L.J.P. Muffler, pp. 37-76, Wiley, Chichester, 1981.

Huyakorn, P.S., and G.F. Pinder, A pressure - enthalpy finite element model for simulating hydrothermal reservoirs, Adv. in Computer Methods for Partial Differential Equations, IMACS, 284-293, 1977.

Jessop, A.M., M.A. Hobart, and J.G. Sclater, The world heat flow data collection - 1975, Geothermal Service of Canada, Geotherm. Ser. 5, 1976.

Kappelmeyer, O., The use of near surface temperature measurements for disscovering anomalies due to causes at depths, Geophys. Prospect., 5(3), 239-258, 1957.

Kappelmeyer, G., and R. Haenel, Geothermics, Gebruder Borntraeger, Berlin, 1974.

Keys, W.S., and R.F. Brown, The use of temperature logs to trace the movement of injected water, Groundwater, 16(1), 32-48, 1978.

Kilty, K., and D.S. Chapman, Convective heat transfer in selected geologic situations, Groundwater, 18(4), 386-394, 1980.

Lachenbruch, A.L., The effect of two-dimensional topography on

surficial thermal gradients, U.S. Geol. Survey, Bull. 1203-E, 1969.

Lachenbruch, A.H., M.L. Sorey, R.E. Lewis, and J.H. Sass, The near surface hydrothermal regime of Long Valley Caldera, J. Geophys. Res., 81, 763-768, 1976.

Lachenbruch, A.H., and J.H. Sass, Heat flow in the United States, in The Earth's Crust, Geophysical Monograph 20, edited by J.G. Heacock, pp.626-675, AGU, Washington, D.C., 1977.

Lewis, T.J., and A.E. Beck, Analysis of heat flow data - detailed observations in many holes in a small area, Tectonophysics, 41, 41-59, 1977.

Li,T.M.C., Axisymmetric numerical simulation of hydrothermal systems including changes in porosity and permeability due to the quartz-water reaction, Ph.D. thesis, The Pennsylvania State University, pp 240, 1980.

Lippmann, M.J., Tsang, C.F., and P.A. Witherspoon, Analysis of the response of geothermal reservoirs under injection and production procedures, SPE 6537, Soc. Petrol. Eng., Dallas, Texas, 1977.

Mansure, A.J., and M. Reiter, A vertical groundwater movement correction for heat flow, J. Geophy. Res., 84(B7), 3490-3496, 1979.

Mercer, J.W., Pinder, G.F., and I.G. Donaldson, A Galerkin finite element analysis of the hydrothermal system at Wairakei New Zealand, J. Geophy. Res., 80(17), 2608-2621, 1975.

Morgan, P., Harder, V., Swanberg, C.A., and P.H. Daggett, A groundwater convective model for Rio Grande Rift geothermal systems, Geothermal Resour. Council, Trans, 5, 193-196, 1981.

Parsons, M.L., Groundwater thermal regime in a glacial complex, Water Resour. Res., 6(6), 1701-1720.

Pinder, G.F., State-of-the-Art Review of Geothermal Reservoir Engineering, Lawrence Berkeley Lab., LBL-9093, 1979.

Pinder, G.F., and W. Gray, Finite element simulation in surface and subsurface hydrology, Academic Press, 1977.

Reiter, M., A.J. Mansure, and C. Shearer, Geothermal characteristics of the Rio Grande rift within the southern Rocky Mountain complex, in Rio Grande Rift: Tectonics and Magmatism, edited by R.E. Reicker, pp. 253-267, AGU, Washington, D.C., 1979.

Ribando, R.J., Torrance, K.E., and D.L. Turcotte, Numerical models for hydrothermal circulation in the oceanic crust, J. Geophy. Res., 81(17), 3007-3012, 1976.

Sauty, J.P., Gringarten, A.C., Menjoz, A., and P.A. Landel,

Sensible energy storage in aquifers 1. Theoretical study, Water Resour. Res., 18(2), 245-252, 1982.

Sauty, J.P., Gringarten, A.C., Fabris, H., Thiery, D., Menjoz, A., and P.A. Landel, Sensible energy storage in aquifers 2. Field experiments and comparisons with theoretical results, Water Resour. Res., 18(2), 253-265, 1982.

Shearer, C., and M. Reiter, Terrestrial heat flow in Arizona, J. Geophys. Res., 86, 6249-6260, 1981.

Sorey, M.L., Measurement of vertical groundwater velocity from temperature profiles in wells, Water Resour. Res., 7(4), 963-970, 1971.

Sorey, M.L., A model of the hydrothermal system of Long Valley caldera, California, Summaries Second Workshop Geothermal Reservoir Engineering, Stanford University, Stanford, California, 324-338, 1976.

Sorey, M.L., Numerical modeling of liquid geothermal systems, USGS Professional Paper 1044-D, 1978.

Stallman, R.W., Notes on the use of temperature data for computing ground water velocity, Societe Hydrotechnique de France, Nancy, France, 6th Assembly on Hydraulics, Rapport 3 question 1 , pp. 1-7, 1960.

Stallman, R.W., Computation of grounndwater velocity from temperature data, in Methods of Collecting and Interpreting Groundwater Data, edited by R. Bentall, U.S. Geol. Surv. Water Supply Pap. 1554-H, 36-46, 1963.

Straus, J.M., and G Schubert, Thermal convection of water in a porous medium: effects of temperature and pressure dependent thermodynamic and transport properties, J. Geophy. Res., 82(2), 325-333, 1977.

Toth, J., A theoretical analysis of groundwater flow in small drainage basins, J. Geophys. Res., 68(16), 4795-4812, 1963.

Tsang, C.F., Buscheck, T., and C. Doughty, Aquifer thermal energy storage: A numerical simulation of Auburn University field experiments, Water Resour. Res., 17(3), 647-658, 1981.

Van Orstrand, C.E., Temperature gradients, in Problems of Petroleum Geology, pp. 989-1021, Am. Ass. Petrol. Geol., Tulsa, Okla., 1934.

Ziagos, J.P., and D.D. Blackwell, A model for the effect of horizontal fluid flow in a thin aquifer on temperature-depth profiles, Trans. Geothermal Resources Council, 5, 221-223, 1981.

FIGURE CAPTIONS

Figure 1. Density and dynamic viscosity of water as a function of temperature.

Figure 2. Finite element grid with segmented water table used in subsequent simulations.

Figure 3. Thermal effects of groundwater flow in a basin of homogeneous isotropic permeability and linear water table. Simulations a, b, and c are carried out for permeabilities 5.0 x 10^{-18} m^2, 2.0 x 10^{-16} m^2, and 5.0 x 10^{-16} m^2 respectively. Heat flow profiles calculated using the upper two nodes in the finite element grid are also shown. Basal heat flux is 60 mW m^{-2}. Parameter values not listed here are given in Table 3.

Figure 4. Temperature depth profile at location D shown in Figure 3-c for the case where permeability is 5.0 x 10^{-16} m^2. Computed heat flow at such a site will depend on depth of investigation in a borehole. Details discussed in text.

Figure 5. Thermal effects of groundwater flow in a basin of isotropic homogeneous permeability and segmented water table. Simulations a, b, and c are carried out for permeabilities 1.0 x 10^{-17} m^2, 3.0 x 10^{-16} m^2, and 8.0 x 10^{-16} m^2, respectively. Heat flow profiles for the three cases are shown at the bottom of the figure. Basal heat flux is 60 mW m^{-2}. Parameter values not listed here are given in Table 3.

Figure 6. Influence of permeability on surface heat flow at the six characteristic sites described in Table 4, case 1 simulations.

Figure 7. Thermal effects of groundwater flow in a basin of anisotropic homogeneous permeability. Horizontal permeability kx is 8.0×10^{-16} m^2; anisotropic ratio kx/kz is 1, 10, and 100 for the three simulations shown.

Figure 8. Influence of anisotropy on the hydrologic disturbance to conductive heat flow in a basin with homogeneous permeability. The quantity dq rms is the root mean square deviation of surface heat flow from the basal flux calculated at all nodes across the finite element grid. A dq rms of near zero corresponds to the conductive case.

Figure 9. Thermal effects of varying the position of a basal low permeability layer. Curve parameters identify depth of this boundary at distance zero on the grid. Permeabilities above and below the boundary are 8.0×10^{-16} m^2 and 1.0×10^{-21} m^2, respectively.

Figure 10. Influence of depth of active flow on the hydrologic disturbance to conductive heat flow. The quantity dq rms is the root mean square deviation of surface heat flow from the basal heat flux calculated at all nodes across the finite element grid. Curve parameters identify depth to low permeability boundary described in Figure 9.

Figure 11. Thermal effects of groundwater flow in a basin with a higher permeability layer at different depths. Layer has thickness 350 m and permeability 1.0 x 10^{-14} m^2. Surrounding medium has permeability 1.0 x 10^{-16} m^2. The top of the aquifer occurs at depths of 2.0 km, 2.65 km and 3.6 km (measured at distance zero on the grid) in simulations a, b, and c respectively. Depth to lower permeability boundary as described in Figure 9 is 4 km.

Figure 12. Influence of aquifer depth, thickness, and permeability contrast on the hydrologic disturbance to conductive heat flow. The quantity dq rms is the root mean square deviation of surface heat flow from the basal heat flux of 60 mW m^{-2} calculated at all nodes across the finite element grid.

Figure 13. Temperature-depth and thermal gradient-depth plots at 3 locations a, b, and c in a basin with an aquifer at a depth of 2 km. (measured at distance zero on grid). The aquifer has thickness 700 m and permeability 1.0 x 10^{-14} m^2. Surrounding medium has permeability 1.0 x 10^{-16} m^2. Depth to lower permeability boundary as described in Figure 9 is 4 km. Porosity is homogeneous with a value 0.05.

Figure 14. Influence of permeability of the medium surrounding an aquifer on the surface heat flow. The aquifer has thickness 350 m and permeability 1.0 x 10^{-14} m^2. The top of the aquifer is at a depth of 2 km. (measured at distance zero on the grid).

Depth to lower permeability boundary as described in Figure 9 is 4 km.

Figure 15. Thermal effects of groundwater flow in a basin with heterogeneous permeability. Shown here are a schematic of the system, the isotherm section, surface heat flow profile, and temperature - depth and thermal gradient - depth plots for locations a, b, and c. The shaded depth interval on the lower plots indicates aquifer location. The lapse rate for the temperature on the water table is -7.0 °C/km.

TABLE CAPTIONS

Table 1. Review of available studies on the thermal effects of groundwater flow. The designation steady state or transient refers to the temperature field. Permeability is classified as homogeneous or heterogeneous and isotropic or anisotropic. The designation viscosity (T) and density (T) refers to incorporation of the temperature dependence of these parameters. The column second from the end classifies the form in which results are presented.

Table 2. Permeability of common geologic media (adapted from Figure 2.4 of Freeze and Cherry, 1979).

Table 3. Parameter values for fluid and thermal properties which are held fixed for all simulations.

Table 4. Characteristic site description for Case 1 simulations.

Table 5. Effect of the water table slope on the extent of the hydrologic disturbance. Values in the body of the table are root mean square deviations of surface heat flow as compared to the basal heat flux. The basin configuration corresponds to the case 1 simulations. The topographic relief on the water table on the upland and lowland slope is 11.5, 17,2, and 25.8 m per km in these simulations. The water table gradient of the slope connecting these two segments is 34.4, 51.6, and 77.3 m per km. Permeability is homogeneous and isotropic.

TABLE 3

Property	Value	
Reference density of fluid	998.2	kgm^{-3}
Specific heat of fluid	4186.0	$J\ kg^{-1}\ °C^{-1}$
Thermal conductivity of fluid	0.58	$W\ m^{-2}\ °C^{-1}$
Thermal conductivty of rock	2.51	$W\ m^{-2}\ °C^{-1}$
Longitudinal dispersivity	100	m
Transverse dispersivity	10	m
Basal heat flux	60	$mW\ m^{-2}$

TABLE 4

Site	Description
A	Upper recharge area
B	Midland of upper slope
C	Above break in the water table slope
D	Toe of the slope
E	Midland of lower slope
F	Lower discharge area

TABLE 5

Permeability (m^2)	Total Relief on Water Table		
	0.67 km	1.0 km	1.5 km
1.0×10^{-16}	5.1	6.9	9.1
3.0×10^{-16}	14.5	19.0	23.5
8.0×10^{-16}	41.2	49.3	54.1

N	authors	date	.123.456.78.9a.bc.de.f.g.hi.	application
1	Bredehoeft & Papadopulos	1965	.x .x .x .x .x . x. . .x	vertical groundwater characteristics
3	Cartwright	1970	.x .x .x .x .x . x. . .x	applied ref.1 to temperature data to estimate discharge for Illinois basin
4	Sorey	1971	.x .x .x .x .x . x. . .x	applied ref.1 to drillhole temperature profiles to estimate velocities and discharge rates
5	Mansure and Reiter	1979	.x .x .x .x .x . x. . .xx	modifies ref.1 to study heat flow variations within single drillhole
6	Domenico & Palciauskas	1965	. x .x .x .x .x . x. . .xx	solution of flow and temperature fields in 2D basin
7	Morgan et al.	1981	. x .x .x .x .x . x. . .xx	applied ref. 6 to Rio Grande rift basins, ivvestigated permeability threshold for advective heat flow effects
10	Cartwright	1971	. x .x . x.x .x .x . . .x	solution for temperatures in confining layer overlying aquifer wth horizontal flow
11	Lewis and Beck	1977	. x . x . x. x.x .x . . .xx	modeled low heat flow pattern caused by down -dip percolation of cold surface waters
12	Keys & Brown	1978	.x .x . x.x .x .x . . .x	applied refs. 8 & 9 to trace injected water in aquifers
13	Kilty & Chapman	1980	. x . x .x . x.x .x .x. . x	modeled heat flow variations by assumed flow in aqiuifers; 3 geologic setings
14	Ziagos & Blackwell	1981	. x .x . x.x. .x .x . . .x	sulution given for transient temperatures in confining beds surrounding horizontal aquifer/fracture
15	Parsons	1970	. x . x .x . x.x . x. . .x	flow and temperatures in a shallow glacial complex
16	Sorey	1976	. x. x. x. x.x . x.x.x.x	temperatures, flow and discharge in Long Valley caldera
16a	Betcher	1977	. x . x.x . x.x . x. . .x	generic modeling of temperature field
17	Andrews	1978	. x . x. x. x.x . x.x.x.x	temperatures in aquifers during heat pump wiater withdrawal/injection
18	Andrews & Anderson	1980	. x. x. x. x.x . x.x.x.x	
19	Smith & Chapman (this pub)	1982	. x . x.x . x. x. x.x.x.xx	generic modeling for thermal regime of basins ,emphasis on sensitivity analysis

Code for table headings

N	number of reference in table
1	1 dimension
2	2 dimension
3	3 dimension
4	analytic solution
5	numerical solution, finite difference
6	numerical solution, finite element
7	steady state
8	transient
9	homogeneous permeability
a	heterogeneous permeability
b	isotropic media
c	anisotropic media
d	flow field assumed 'a priori'
e	flow field calculated; coupled solution
f	temperature dependent density
g	temperature dependent viscosity
h	form of results: temperature field
i	form of results: heat flow profile

This table is being drafted. Final copy will be submitted when ready.

Table 21

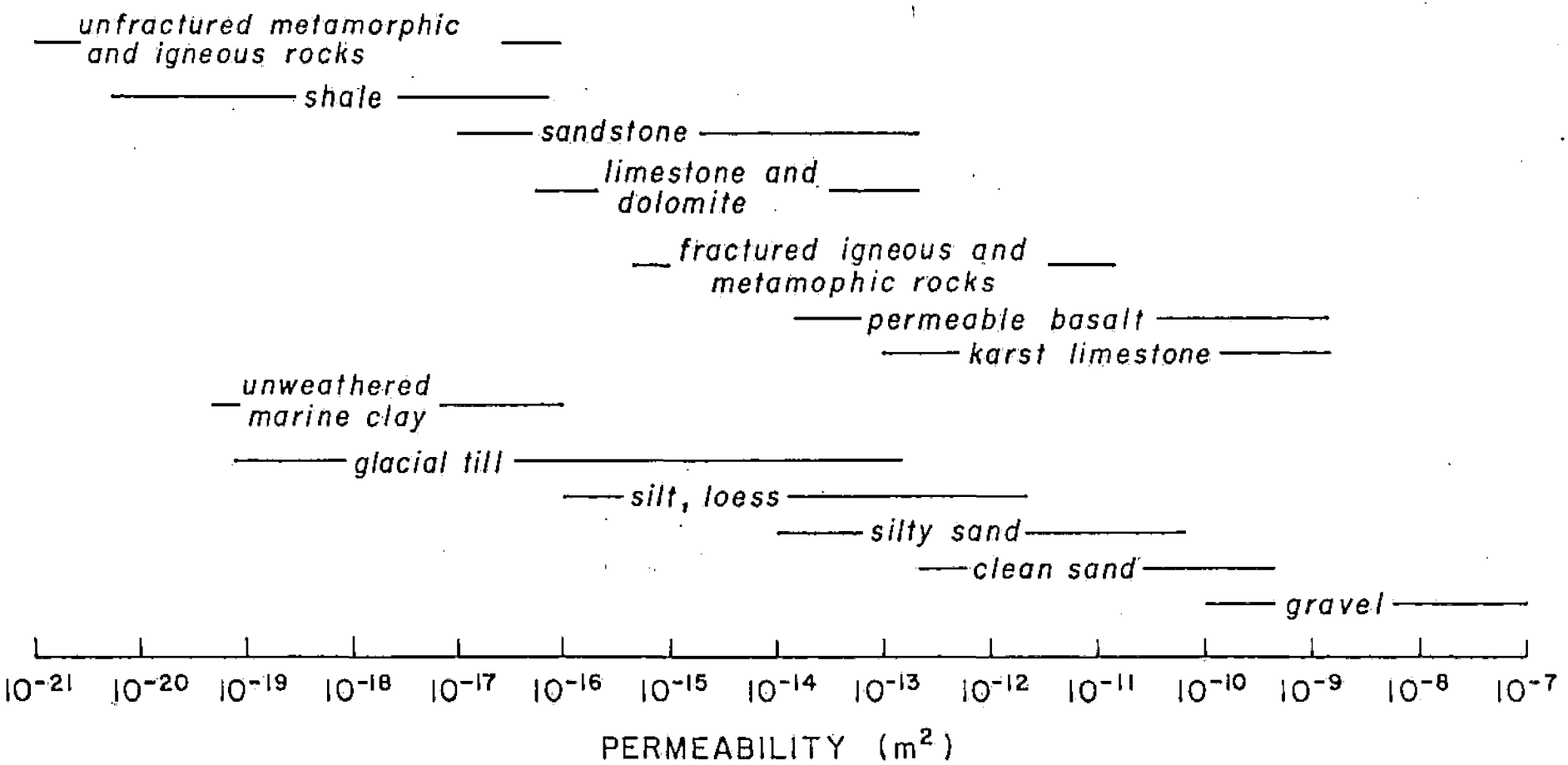
unfractured metamorphic and igneous rocks
shale
sandstone
limestone and dolomite
fractured igneous and metamophic rocks
permeable basalt
karst limestone
unweathered marine clay
glacial till
silt, loess
silty sand
clean sand
gravel
10-21 10-20 10-19 10-18 10-17 10-16 10-15 10-14 10-13 10-12 10-11 10-10 10-9 10-8 10-7
PERMEABILITY (m2)

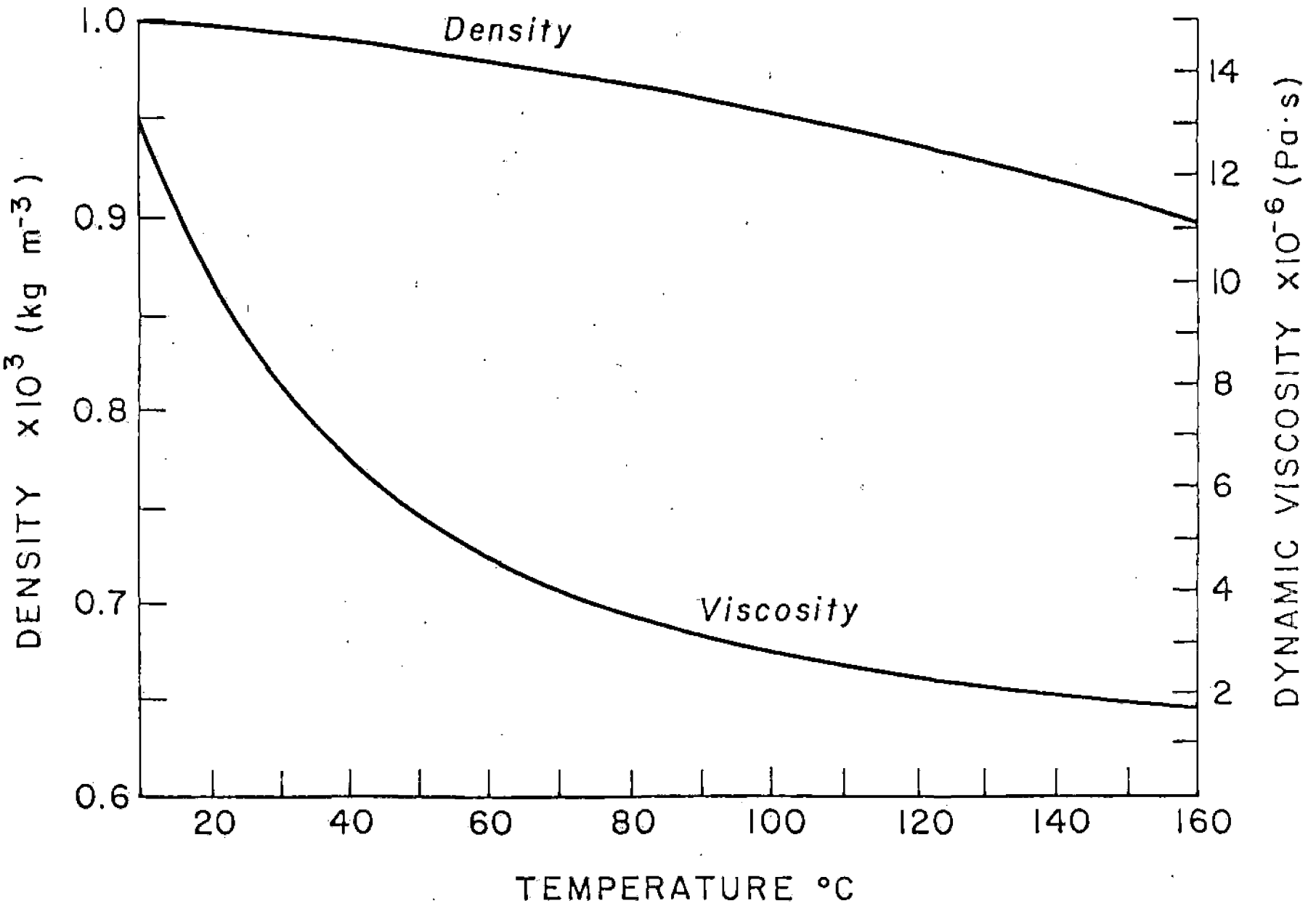
Density
Viscosity
1.0
0.9
0.8
0.7
0.6
DENSITY X10³ (kg m⁻³)
14
12
10
8
6
4
2
DYNAMIC VISCOSITY X10⁻⁶ (Pa·s)
20
40
60
80
100
120
140
160
TEMPERATURE °C

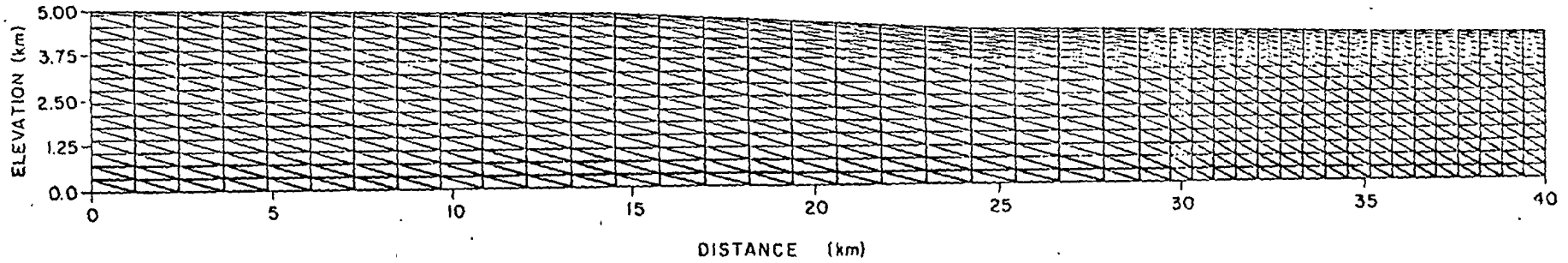
5.00
3.75
2.50
1.25
0.0
ELEVATION (km)
0
5
10
15
20
25
30
35
40
DISTANCE (km)

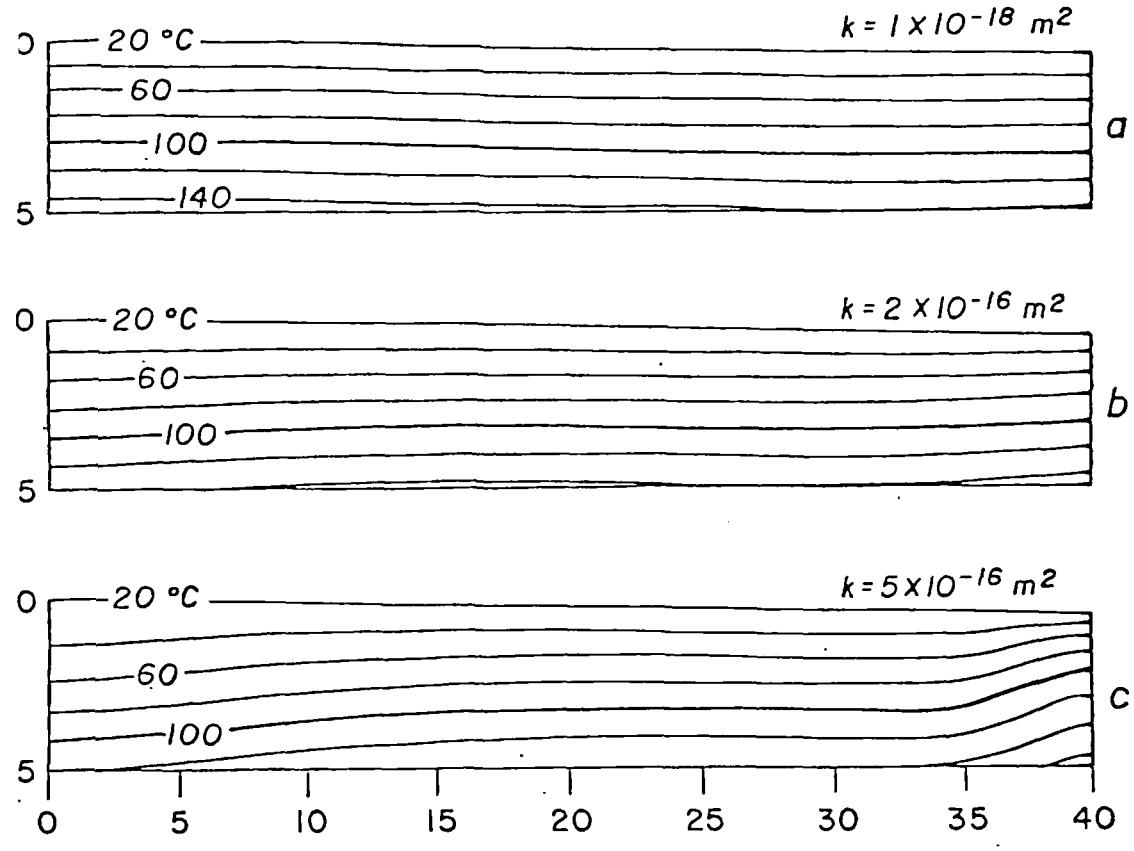
k = 1 X 10⁻¹⁸ m²
20 °C
60
100
140
a
k = 2 X 10⁻¹⁶ m²
20 °C
60
100
b
k = 5 X 10⁻¹⁶ m²
20 °C
60
100
c
0
5
0
5
10
15
20
25
30
35
40
DISTANCE (km)

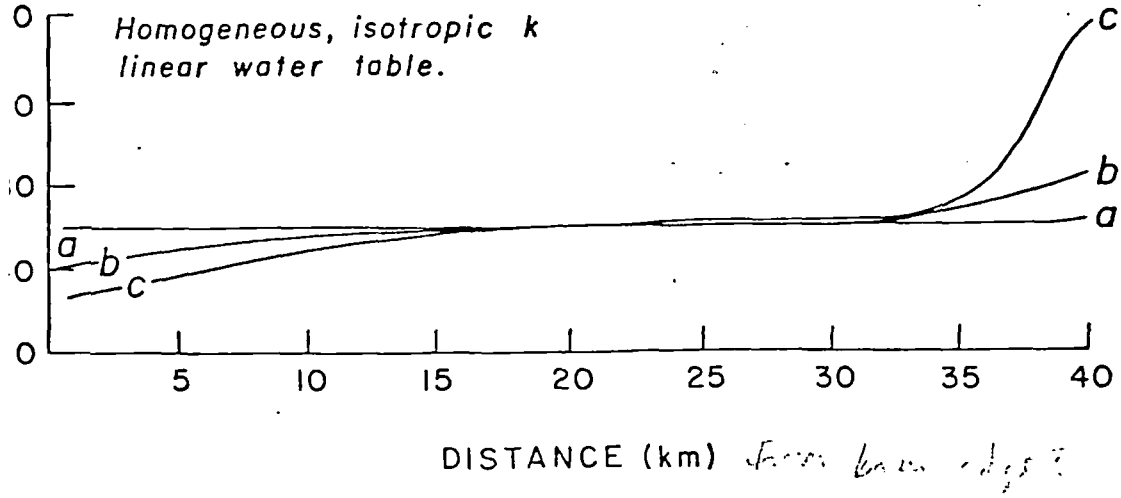
Homogeneous, isotropic k
linear water table.
a
b
c
5
10
15
20
25
30
35
40
DISTANCE (km)

Fig 3

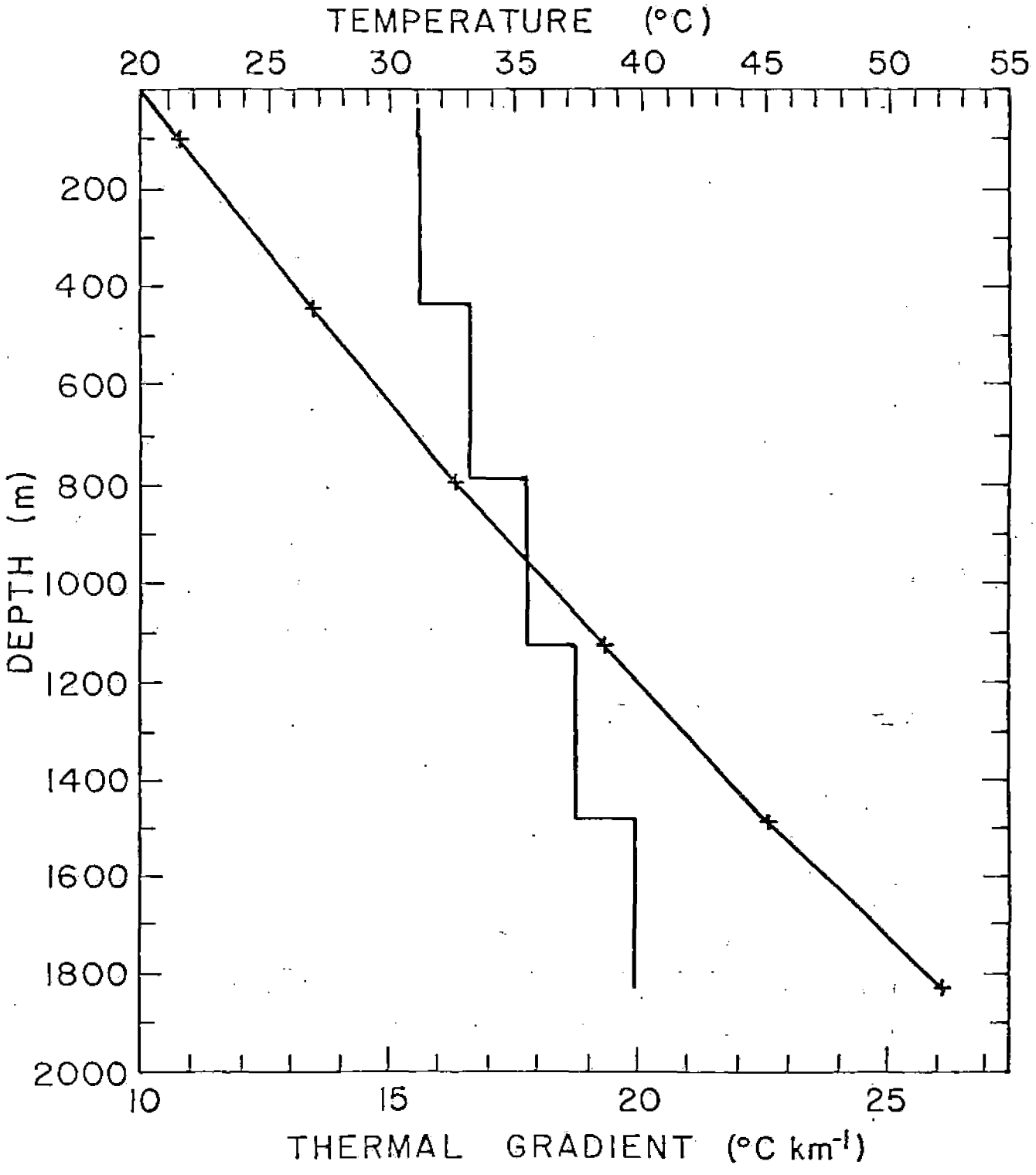
TEMPERATURE (°C)
20
25
30
35
40
45
50
55
DEPTH (m)
200
400
600
800
1000
1200
1400
1600
1800
2000
10
15
20
25
THERMAL GRADIENT (°C km⁻¹)

Fig 4

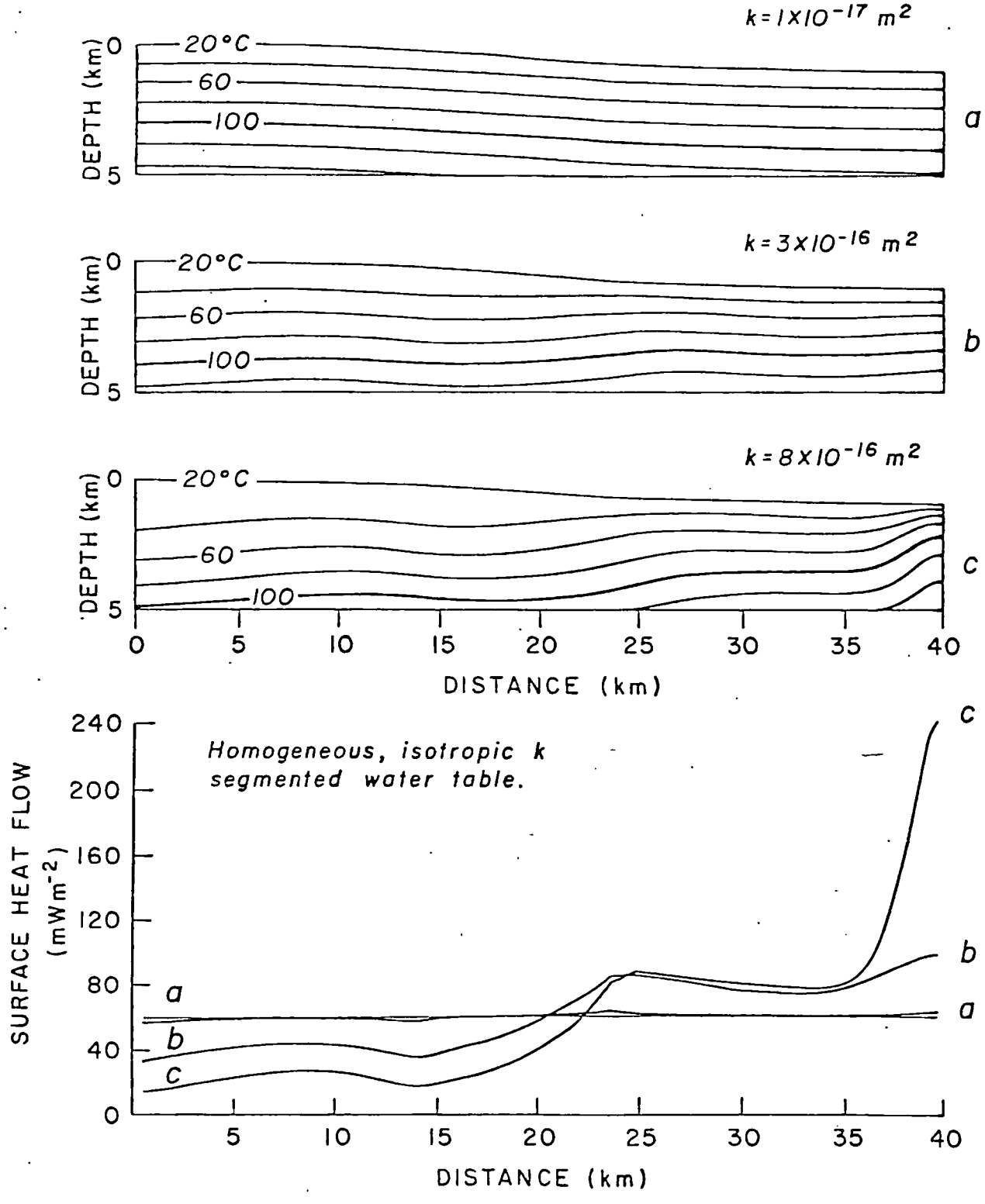
k = 1X10⁻¹⁷ m²
DEPTH (km)
0
5
20°C
60
100
a
k = 3X10⁻¹⁶ m²
b
k = 8X10⁻¹⁶ m²
c
0
5
10
15
20
25
30
35
40
DISTANCE (km)
SURFACE HEAT FLOW (mWm⁻²)
240
200
160
120
80
40
0
Homogeneous, isotropic k
segmented water table.
DISTANCE (km)

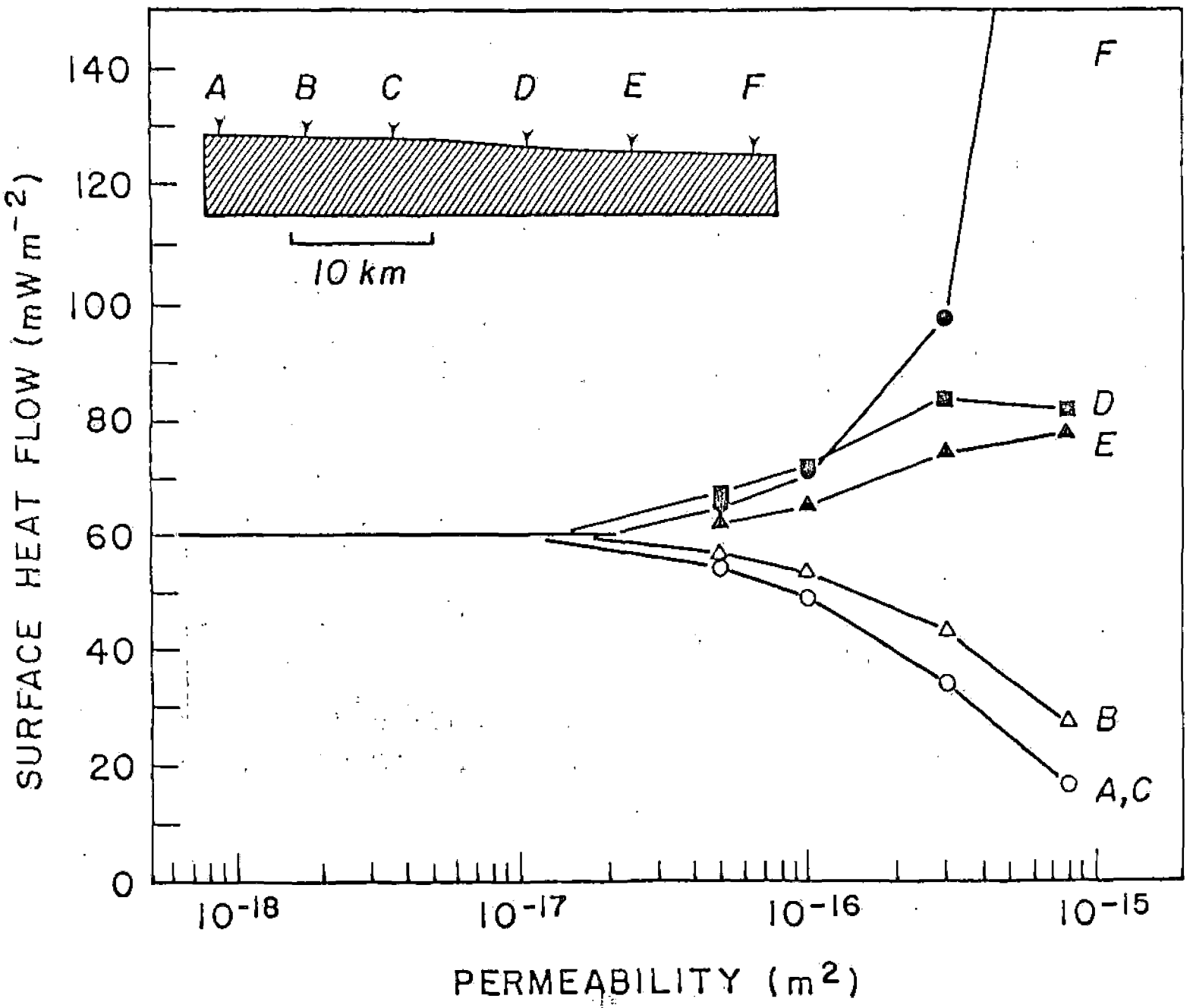
A
B
C
D
E
F
10 km
140
120
100
80
60
40
20
0
SURFACE HEAT FLOW (mW m^{-2})
F
D
E
B
A,C
10^{-18}
10^{-17}
10^{-16}
10^{-15}
PERMEABILITY (m^2)

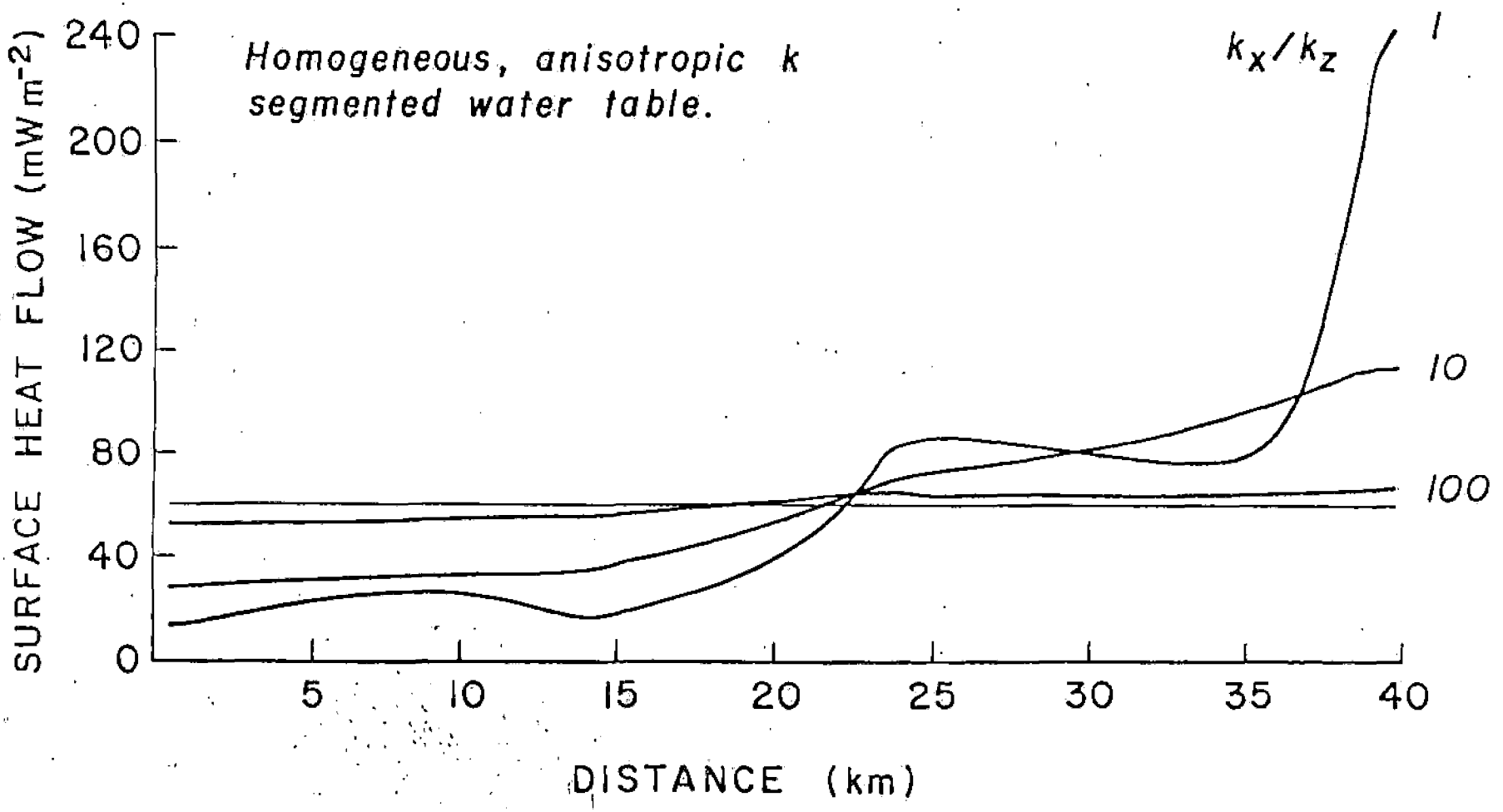
Homogeneous, anisotropic k
segmented water table.
k_x/k_z
1
10
100
SURFACE HEAT FLOW ($mW\,m^{-2}$)
240
200
160
120
80
40
0
5
10
15
20
25
30
35
40
DISTANCE (km)

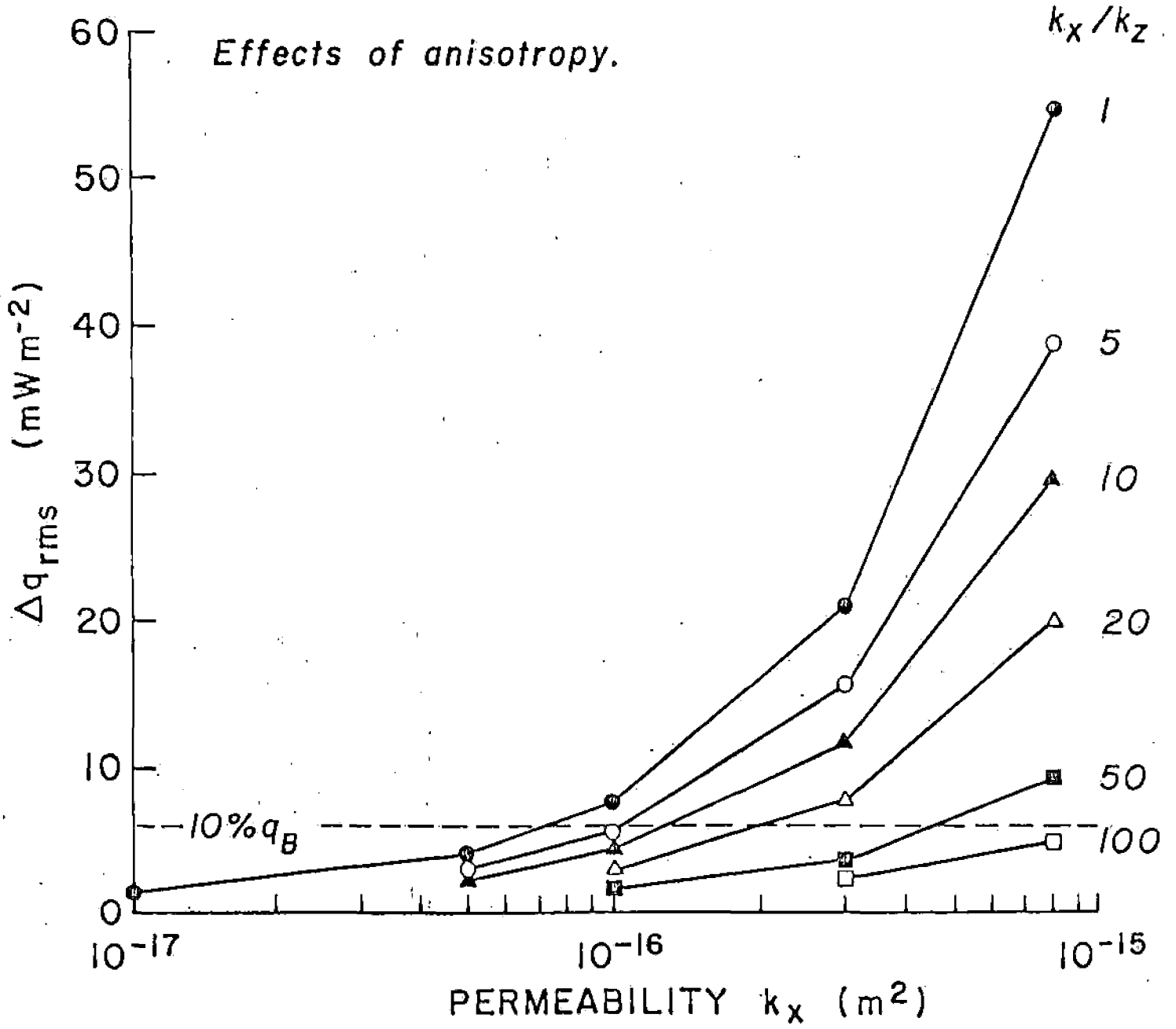
Effects of anisotropy.
k_x/k_z
1
5
10
20
50
100
60
50
40
30
20
10
0
Δq_{rms} (mW m^{-2})
10%q_B
10^{-17}
10^{-16}
10^{-15}
PERMEABILITY k_x (m^2)

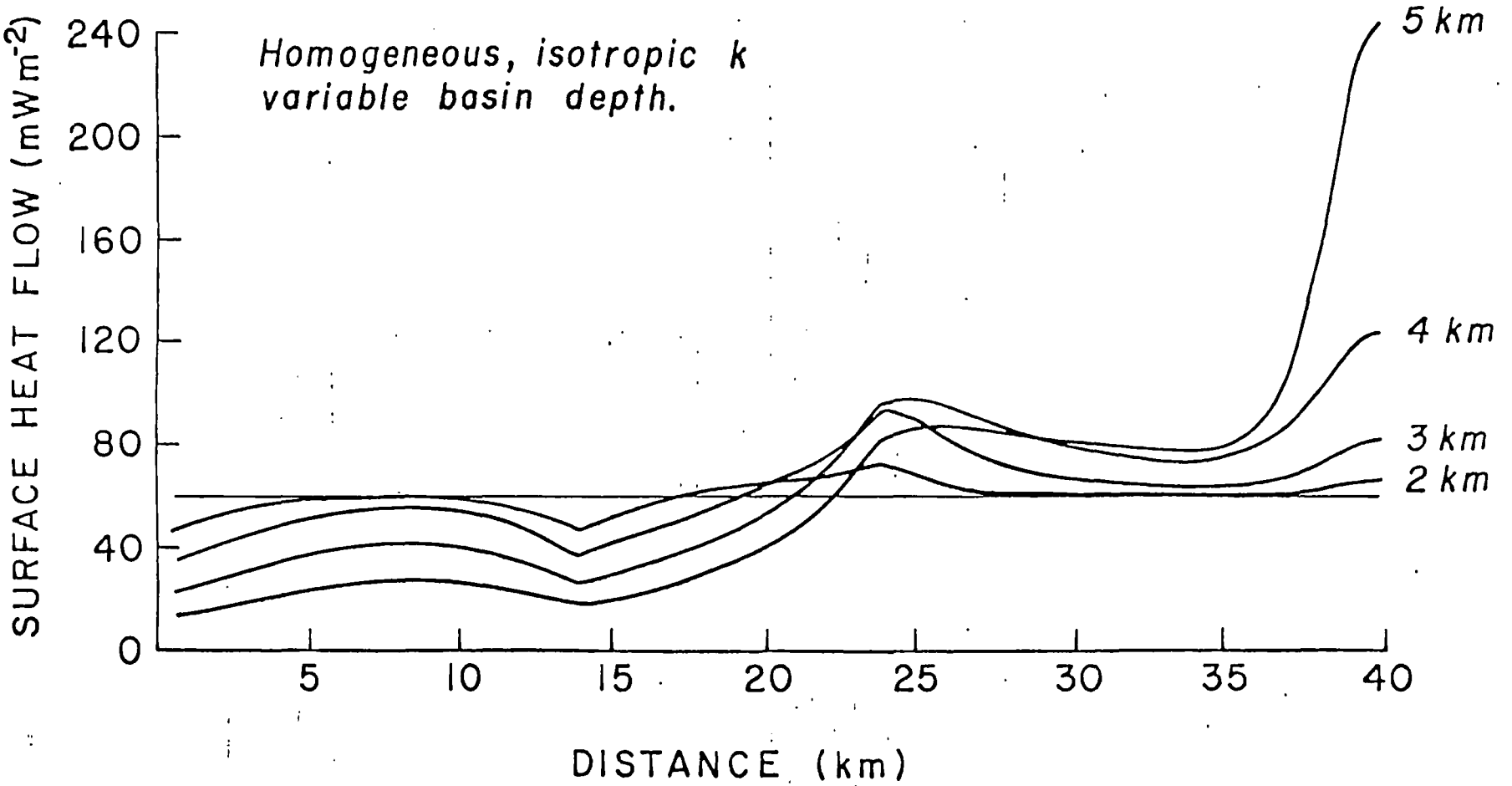
Homogeneous, isotropic k
variable basin depth.
SURFACE HEAT FLOW (mWm-2)
240
200
160
120
80
40
0
5
10
15
20
25
30
35
40
DISTANCE (km)
5 km
4 km
3 km
2 km

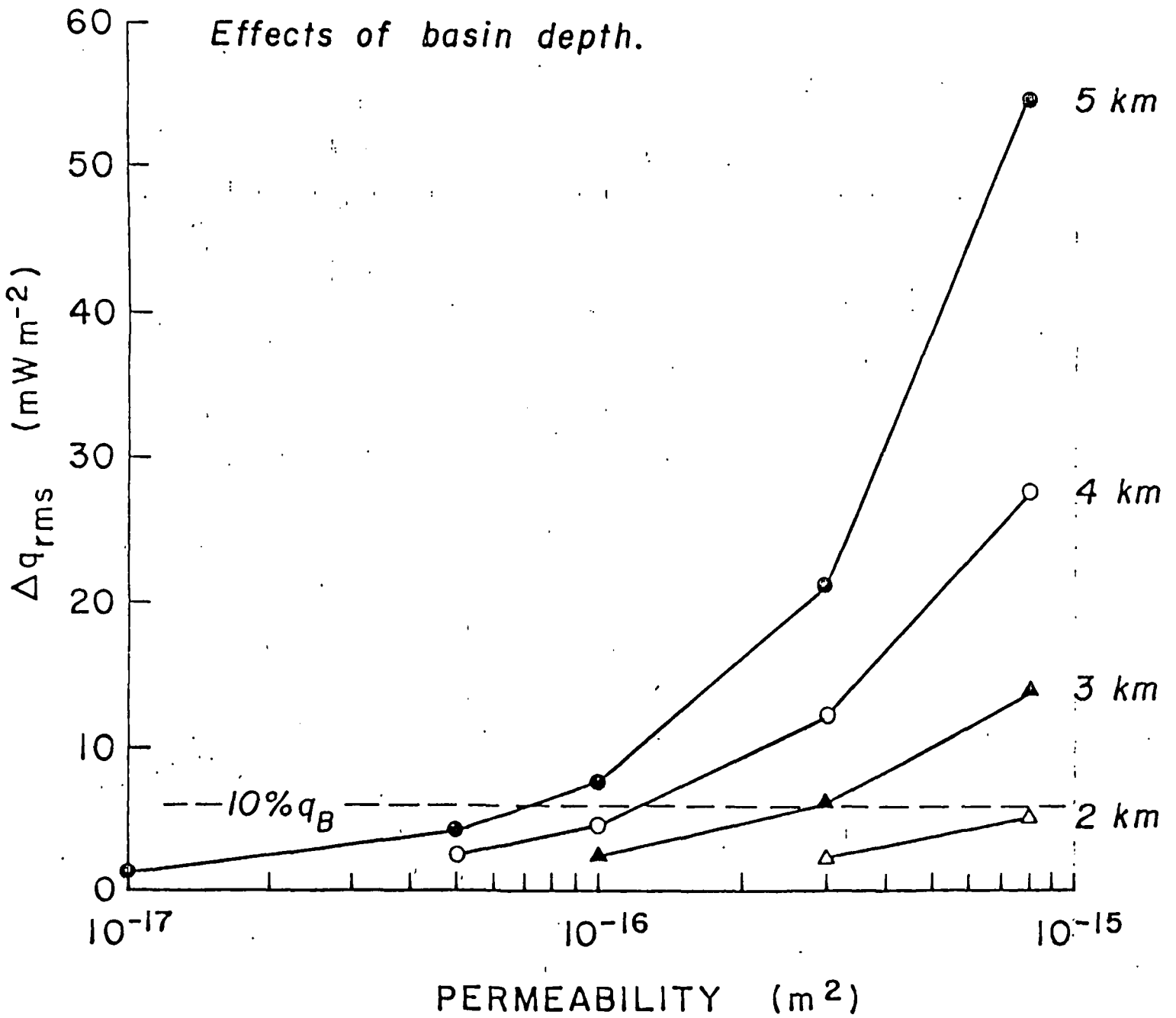
Effects of basin depth.
60
50
40
30
20
10
0
Δq_{rms} (mW m^{-2})
5 km
4 km
3 km
2 km
$10\% q_B$
10^{-17}
10^{-16}
10^{-15}
PERMEABILITY (m^2)

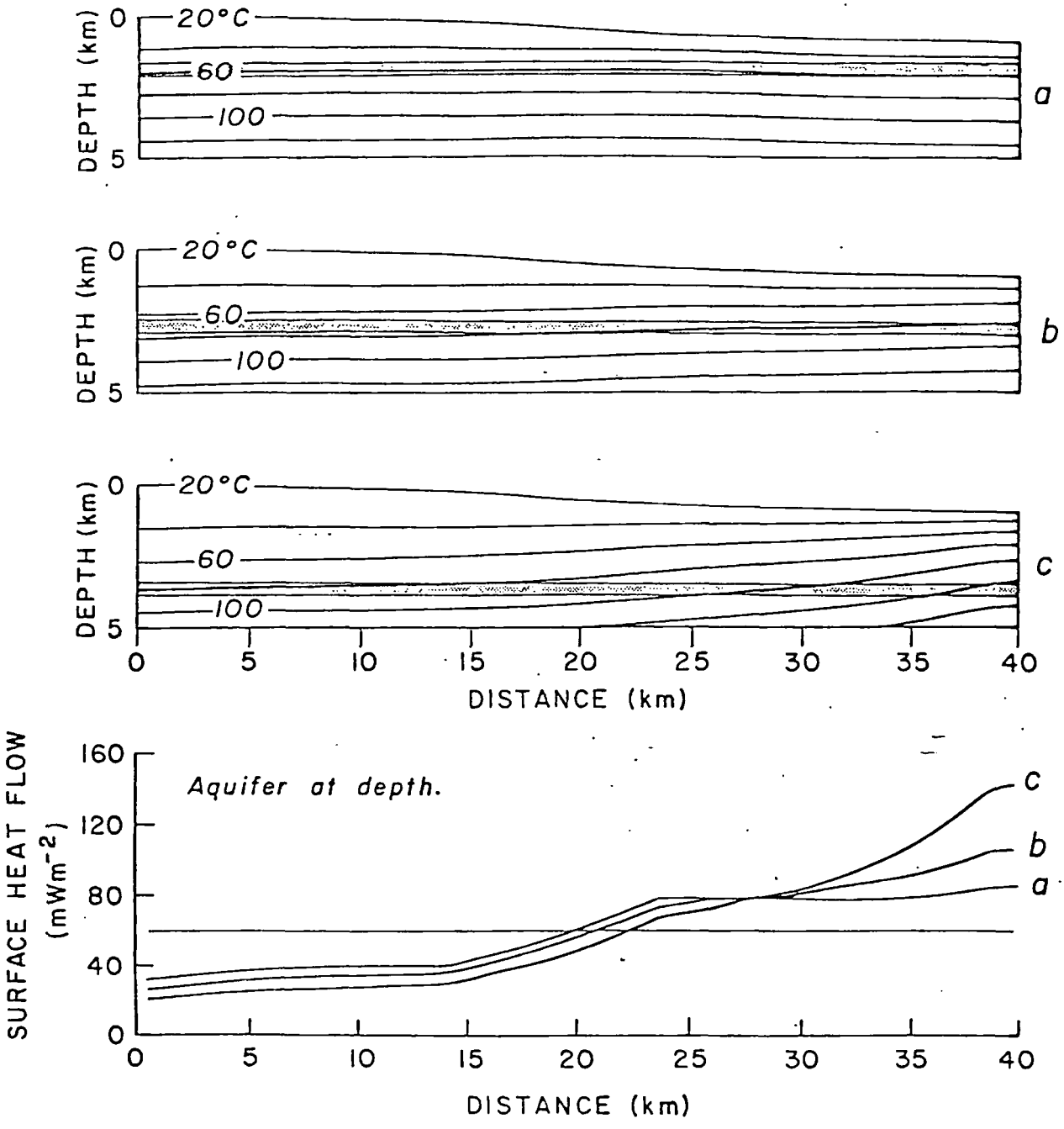
DEPTH (km)
0
5
20°C
60
100
a
b
c
0
5
10
15
20
25
30
35
40
DISTANCE (km)

SURFACE HEAT FLOW
(mWm⁻²)
160
120
80
40
0
Aquifer at depth.
c
b
a
0
5
10
15
20
25
30
35
40
DISTANCE (km)

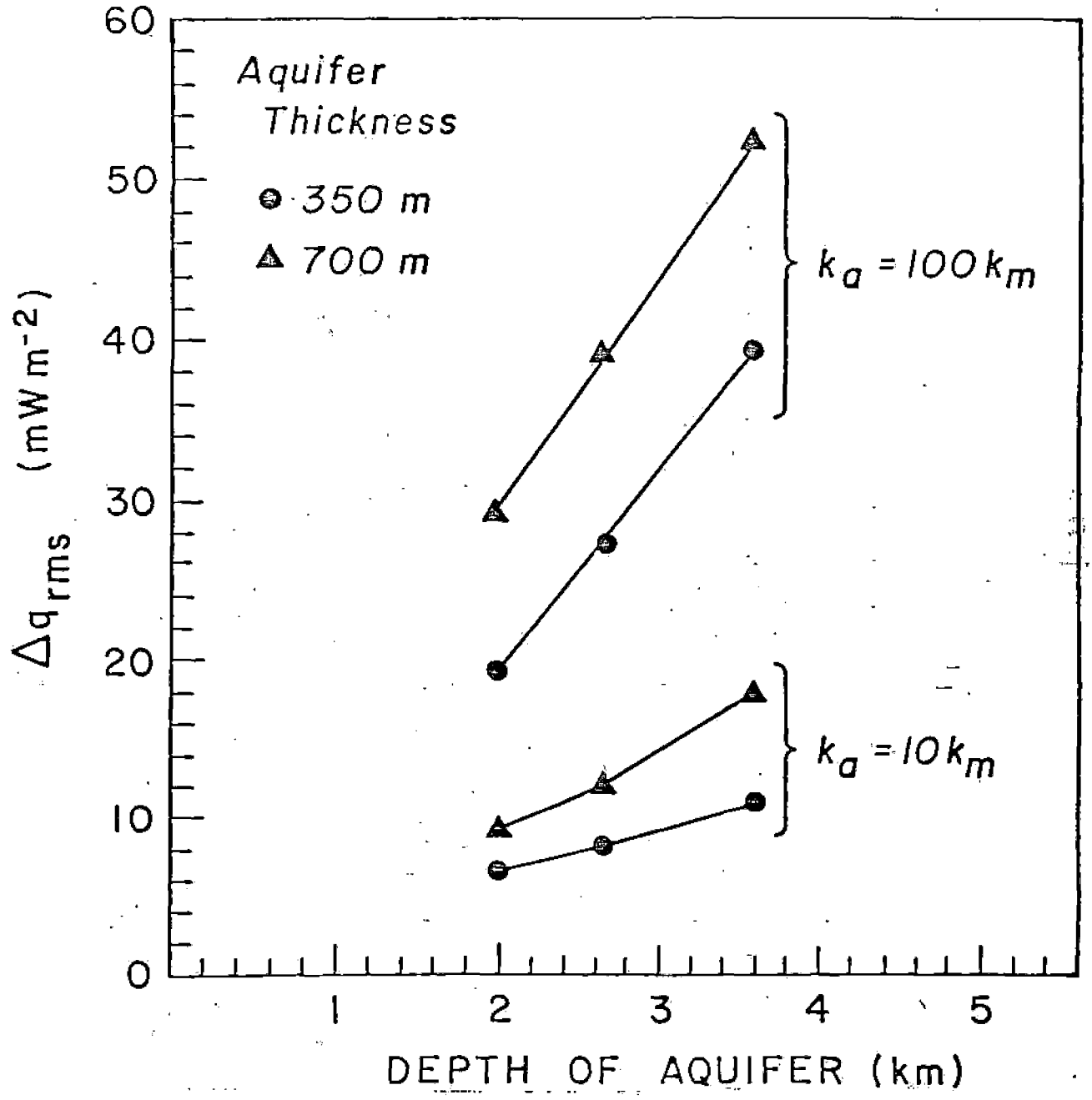
Aquifer
Thickness
350 m
700 m
$k_a = 100\,k_m$
$k_a = 10\,k_m$
Δq_{rms} (mW m^{-2})
60
50
40
30
20
10
0
1
2
3
4
5
DEPTH OF AQUIFER (km)

Fig 1

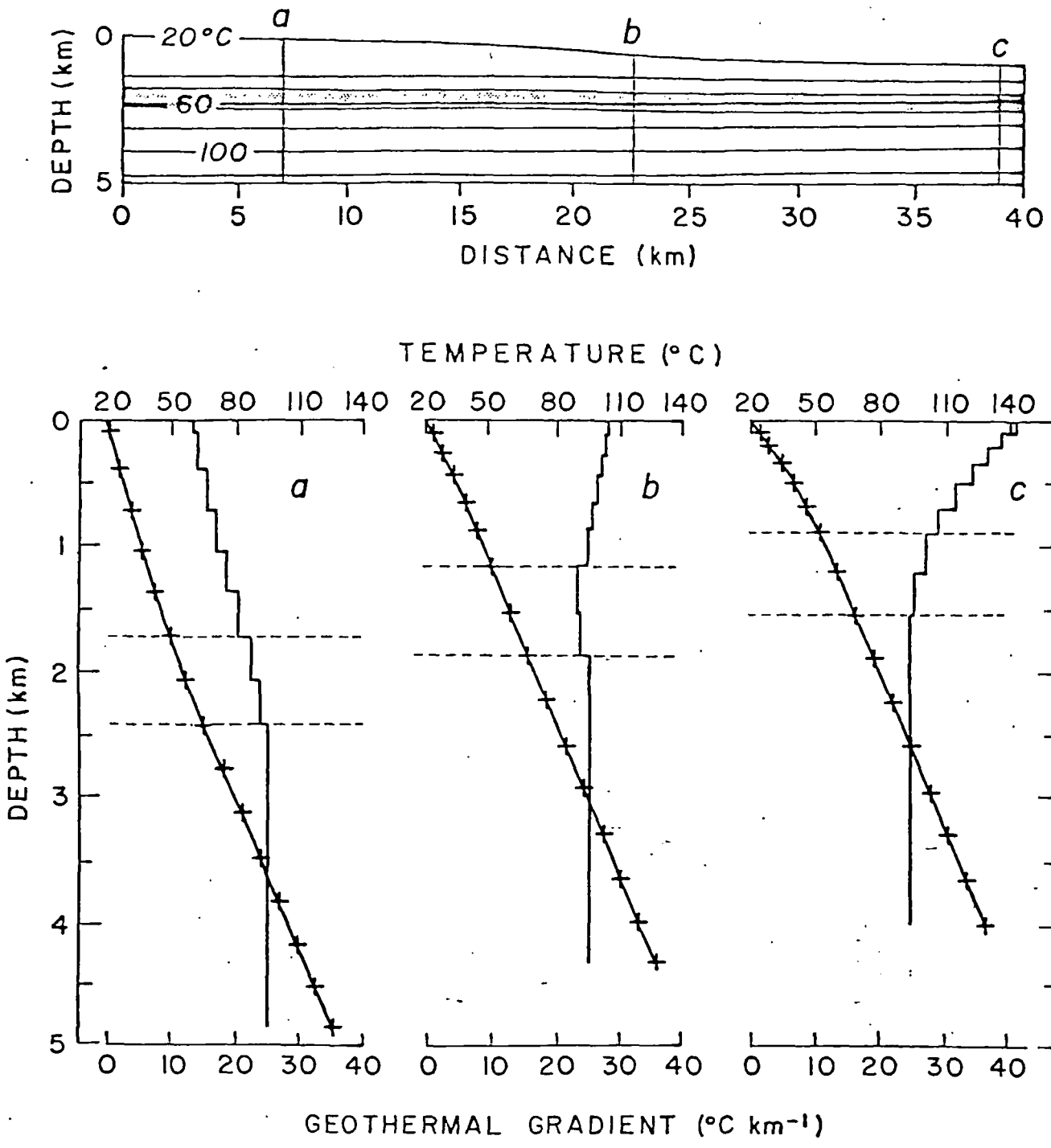
a
b
c
20°C
60
100
DEPTH (km)
0
5
0
5
10
15
20
25
30
35
40
DISTANCE (km)
TEMPERATURE (°C)
20 50 80 110 140
0
1
2
3
4
5
DEPTH (km)
0 10 20 30 40
GEOTHERMAL GRADIENT (°C km⁻¹)

Fig 13

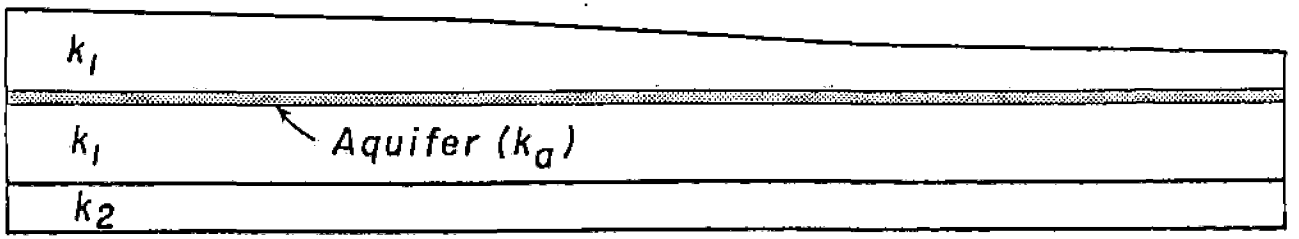
k_1
k_1
Aquifer (k_a)
k_2

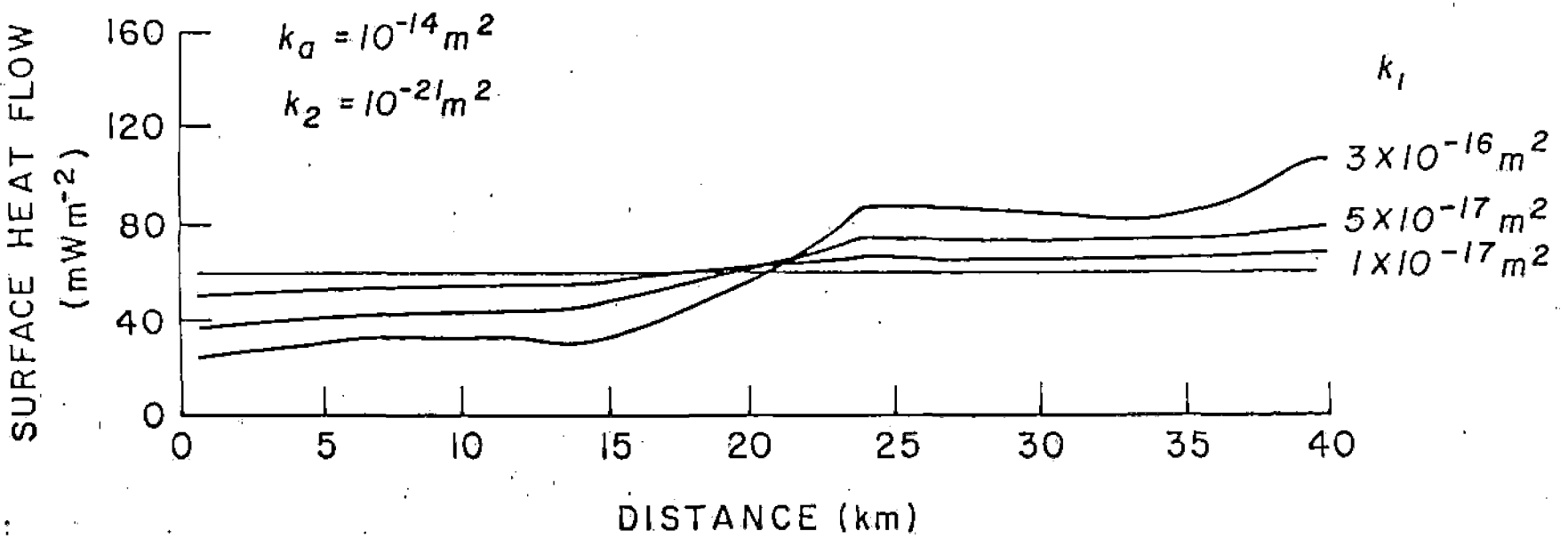
$k_a = 10^{-14} m^2$
$k_2 = 10^{-21} m^2$
k_1
$3 \times 10^{-16} m^2$
$5 \times 10^{-17} m^2$
$1 \times 10^{-17} m^2$
SURFACE HEAT FLOW ($mW m^{-2}$)
160
120
80
40
0
0
5
10
15
20
25
30
35
40
DISTANCE (km)

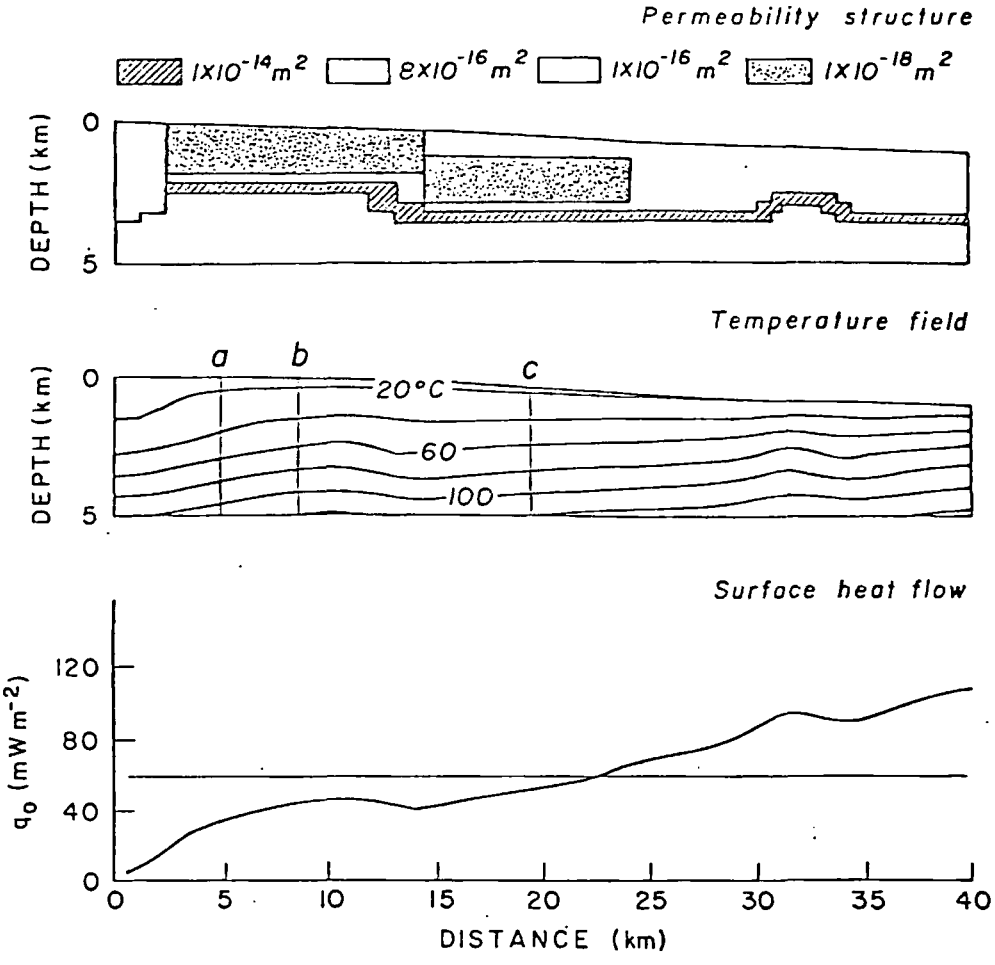
Permeability structure
1X10⁻¹⁴m²
8X10⁻¹⁶m²
1X10⁻¹⁶m²
1X10⁻¹⁸m²
DEPTH (km)
0
5
Temperature field
a
b
c
20°C
60
100
DEPTH (km)
Surface heat flow
q₀ (mW m⁻²)
120
80
40
0
0 5 10 15 20 25 30 35 40
DISTANCE (km)

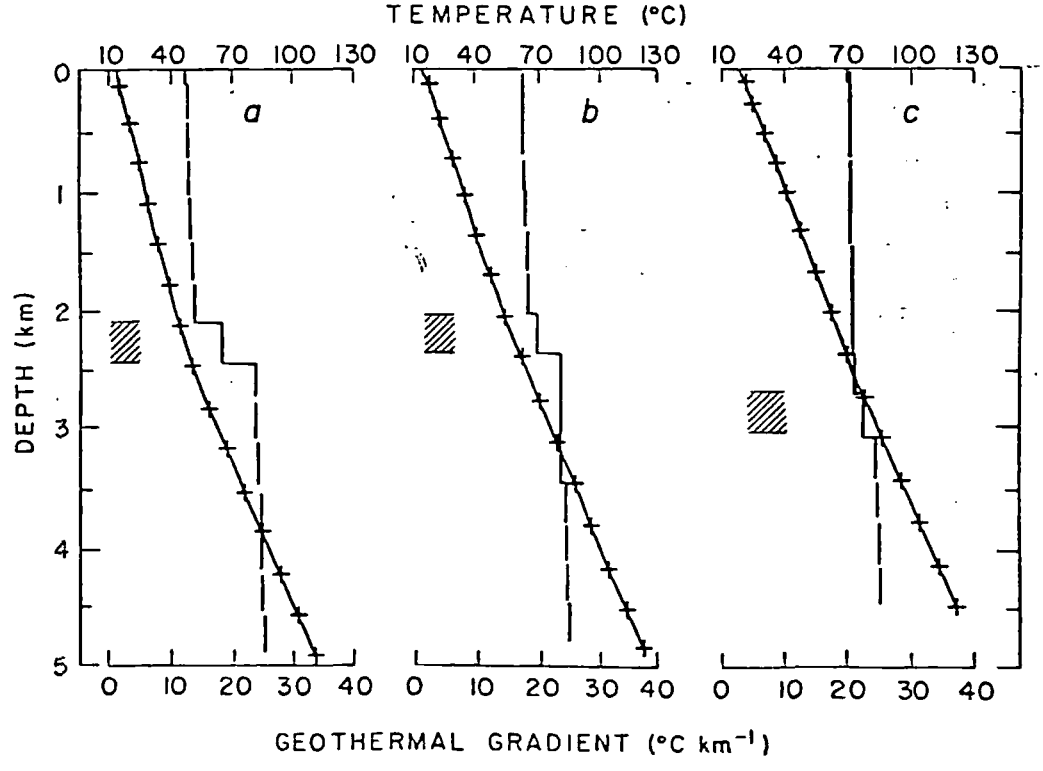
TEMPERATURE (°C)
10 40 70 100 130
a
b
c
DEPTH (km)
0
1
2
3
4
5
0 10 20 30 40
GEOTHERMAL GRADIENT (°C km⁻¹)

Fig. 15